2011-07-08

Spinal Implant with Customized and Non-Linear Stiffness

Eric Ray Dodgen
Brigham Young University - Provo

Spinal Implant with Customized and Non-Linear Stiffness

Eric R. Dodgen

A thesis submitted to the faculty of
Brigham Young University
in partial fulfillment of the requirements for the degree of

Master of Science

Larry L. Howell, Chair
Anton E. Bowden
Mark B. Colton

Department of Mechanical Engineering

Brigham Young University

June 2011

ABSTRACT

Spinal Implant with Customized and Non-Linear Stiffness

Eric R. Dodgen
Department of Mechanical Engineering, BYU
Master of Science

There is a need for spinal implants that have nonlinear stiffness to provide stabilization if the spine loses stiffness through injury, degeneration, or surgery. There is also a need for spinal implants to be customizable for individual needs, and to be small enough to be unobtrusive once implanted. Past and ongoing work that defines the effects of degeneration on the torque rotation curve of a functional spinal unit (FSU) were used to produce a spinal implant which could meet these requirements.

This thesis proposes contact-aided inserts to be used with the FlexSuRe™ spinal implant to create a nonlinear stiffness. Moreover, different inserts can be used to create customized behaviors. An analytical model is introduced for insert design, and the model is verified using a finite element model and tests of physical prototypes both on a tensile tester and cadaveric testing on an in-house spine tester. Testing showed the inserts are capable of creating a non-linear force-deflection curve and it was observed that the device provided increased stiffness to a spinal segment in flexion-extension and lateral-bending.

This thesis further proposes that the FlexSuRe™ spinal implant can be reduced in size by joining LET joint geometries in series in a serpentine nature. An optimization procedure was performed on the new geometry and feasible designs were identified. Moreover, due to maintaining LET joint geometry, the contact-aided insert could be implemented in conjunction with this new device geometry.

Keywords: spinal implant, dynamic stabilization, motion restoration, disc degeneration, lumbar spine, motion restoration, disc decompression

ACKNOWLEDGMENTS

As is true with all things in life, the cooperation of many individuals made the work presented in this thesis possible. Special thanks are extended to my graduate committee Dr. Howell, Dr. Bowden and Dr. Colton, who greatly influenced, motivated, and made this work possible.

I would also like to recognize a few of my of research colleagues who greatly contributed to this work. Eric Stratton and Peter Halverson were among the initial designers of the Flex-SuRe™ and developed many tools and models which have been used during the further development of the device. D. Keith Stolworthy and Shannon Zirbel were closely involved with the development of the device as well as the research. They pioneered the research regarding the effects of degeneration on the lumbar spine. They also developed the Spine tester as well as testing methodology and data analysis methods for the data collected. Their research was integral to this work and its development. Thanks are extended to all the individuals involved with the Compliant Mechanisms Research group (CMR), the Brigham Young University Applied Biomechanics Engineering Laboratory (BABEL) and the Compliant Mechanism -Spine group.

The optimization presented in this work was adapted from a class project, and Chapter 6 was largely taken from the report done on that class project. I would like to thank my teammate Justin Black for his contributions to both the optimization process and the writing of the class report.

The financial support of Crocker Spinal Technologies, Inc. is gratefully acknowledged, as well as their support in acquiring surgeon feedback for the development of the device. The financial support of the Utah Technology Commercialization and Innovation Program and the BYU Technology Transfer Design Fund are also acknowledged.

I would also like to express my most heart felt gratitude to my dear wife Lea who has always supported me and stood by me.

TABLE OF CONTENTS

LIST OF TABLES . . . . . **vi**

LIST OF FIGURES . . . . . **viii**

Chapter 1 Background **1**
1.1 Research Objectives 1
1.2 Problem Statement 1

Chapter 2 Effects of Degeneration on the Torque Rotation Curve of a Functional Spinal Unit **5**
2.1 Design Requirements 5
2.2 Establishing the Necessity of a Study Which Fully Defines the Effects of Degeneration 7
2.2.1 Necessary Criteria to be Met 7
2.2.2 Studies That Present Significant Data 9

Chapter 3 Design of a Spinal Implant with Customizable and Nonlinear Stiffness . . **15**
3.1 Objective 15
3.2 Methods 15
3.2.1 Concept Generation and Selection 17
3.2.2 Modeling Top Concepts 22
3.2.3 Design and Geometry of Contact-Aided Attachment 26

Chapter 4 Modeling and Testing of the Spinal Implant **29**
4.1 Introduction 29
4.2 Models 30
4.2.1 Analytical Model 30
4.2.2 Finite Element Model 36
4.3 Physical Testing 37
4.3.1 Set Up 38
4.4 Discussion of Results 39

Chapter 5 Cadaveric Testing on a Custom-Built Spine Tester **41**
5.1 Introduction 41
5.2 Set Up and Procedure 41
5.3 Results 43

Chapter 6 Development of the SPAR by Reducing Device Size Through Geometric Optimization **51**
6.1 Introduction 51
6.2 Set Up 52
6.3 Procedure 54

6.4 Results of Three Optimization Scenarios 56

Chapter 7 Conclusion and Recommendations 59

REFERENCES 63

Appendix A ANSYS Batch File For Contact-Aided Model 69

Appendix B Mathematica Code for Contact-Aided Model 75

B.1 Ellipse Defined 75
B.2 Contact-Aided Cantilevered Beam 75
B.3 No Contact Cantilevered Beam 78

Appendix C ANSYS Batch File For Optimization 81

LIST OF TABLES

2.1 Design requirements and definitions 8

3.1 Material properties used during modeling of concepts 22
3.2 Spinal segment rotation at input torques for various lengths and thicknesses 23
3.3 Flexure and contact surface dimensions 24

5.1 Fit values for flexion-extension data 43
5.2 Fit values for lateral-bending data 43
5.3 Fit values for axial-rotation data 45
5.4 Comparison of fit values for flexion-extension data with respect to natural disc . . . 47
5.5 Comparison of fit values for Lateral-bending data with respect to natural disc . . . 48
5.6 Comparison of fit values for axial-rotation data with respect to natural disc 49

6.1 Analysis and design variables, analysis and design functions. 54
6.2 Optimums found using two starting point acquisition methods. 56
6.3 Optimized designs from differing objectives. 58

7.1 Evaluation of FlexuRe™ According to Functional Requirements 60

LIST OF FIGURES

1.1 Prototype of the FlexSuRe™ 2
1.2 Torque rotation curve correction 4

2.1 Flexion-extension torque rotation of the degenerated upper lumbar spine 10
2.2 Flexion-extension torque rotation of the degenerated upper lumbar spine 11
2.3 Axial torque rotation of the degenerated lumbar spine 12
2.4 Effects of disc degeneration on segmental motion 14

3.1 FlexSuRe™ definitions 16
3.2 Customizable via press fit 17
3.3 Customizable via lead screw 18
3.4 Pre-compressing using a screw 18
3.5 Pre-stressing using moment end loads 18
3.6 Pre-torquing using adjustment and set screws 19
3.7 Variable cross-sectional area 19
3.8 Adding multiple flexure design 20
3.9 Adding flexures during actuation 21
3.10 Multiple flexures with variable lengths 21
3.11 Contact-aided flexure shown deflected on a circular contact profile. 21
3.12 Contact-aided flexure and two different contact profiles 22
3.13 FlexSuRe™ and contact surface dimensions defined 24
3.14 Displacement profiles of contact-aided and non-contact-aided flexures 25
3.15 Displacement curves for closed form solution and ANSYS solution 25
3.16 Force displacement profiles 26
3.17 Contact-aided attachment for FlexSuRe™ 27

4.1 Interaction of the FlexSuRe™ with the contact surfaces 31
4.2 The general flexible beam 35
4.3 Force versus displacement curves for analytical and FEA data. 36
4.4 Stress versus displacement curves for analytical and FEA data. 37
4.5 Comparison of displacements by different models 38
4.6 Prototype to be tested 39
4.7 Test data, analytical and FEA results 40

5.1 Flexion-extension data and curve fit 44
5.2 Lateral-bending data and curve fit 45
5.3 Axial-rotation data and curve fit 46
5.4 Flexion-extension curve fits compared 47
5.5 lateral-bending curve fits compared 48
5.6 Axial-rotation curve fits compared 48
5.7 Axial-rotation raw data overlaid using gray scale differentiation. 49

6.1 Serpentine geometry defined 53
6.2 Design space contour plots 55

6.3 NX Nastran visualization verifying ANSYS results 56
6.4 Optimized designs compared geometrically 57

CHAPTER 1. BACKGROUND

1.1 Research Objectives

The objective of this research is to model, test, and increase the compatibility and customizability of a spinal implant. This will result in a spinal implant that incorporates a bio-friendly geometric design, is bio-compatible, has infinite life in fatigue, avoids creep and stress relaxation, and can be calibrated for the individual patient. These objectives need to be met while maintaining the ability to correct the degenerated FSU's force-deflection curve to a pre-degenerative state.

1.2 Problem Statement

Chronic back pain is a common debilitating condition [1]. Causes of chronic back pain vary widely, however, three major causes are Spondylolisthesis, Degenerative Disc Disease (DDD), and Spinal Stenosis. Current treatments for these conditions include non-surgical approaches (e.g. physical therapy, pharmaceutical), and invasive surgeries (e.g. minimally invasive discectomy, spinal fusion) [2]. The current surgical procedures for this condition remove tissue to eliminate or reduce the pain [2]. Recent studies have been aimed at providing less invasive alternatives to these treatments [2]. Dynamic stabilization systems for the functional spinal unit are one such technology [3]. Dynamic stabilization systems are meant to stabilize the degenerated portion of the spine by restricting motion. Although this approach stabilizes the spine it also eliminates necessary motion.

The inter-vertebral disc (IVD) is a cartilaginous mass of collagen fibers and lamellae. There are few blood vessels within the IVD; therefore, it relies on diffusion and bulk fluid flow to get the nutrients it needs [4, 5]. To address this issue of nutrition, a system would be preferred which can stabilize and restore the motion of the FSU to a pre-degenerated state.

Figure 1.1: Prototype of the FlexSuRe™

The FlexSuRe™ spinal implant is similar to dynamic stabilization systems in that it can provide stability to the spine. However it is also different in that its purpose is not to restrict motion but provide a force-deflection curve capable of re-stabilizing the spine and returning it to healthy motion [6]. The condition of stability and healthy motion will likely relieve pain and aid in the recovery process because healthy motion helps the inter-vertebral disc (IVD) get nutrients while preventing over extension of soft tissues. Further development of the FlexSuRe™ will include a bio-friendly geometry and a bio-compatible material while incorporating the capability of having the force-deflection curve altered to attain a tailored stiffness. An image of a FlexSuRe™ prototype is shown in Figure 1.1.

A mathematical model was developed for the FlexSuRe™ to show how the implant would correct the degenerated FSU and return it to a healthier state [6]. Figure 1.2 shows an image from this model and how the device corrects the degenerative state by restoring the needed stiffness to the FSU. However, the healthy and degenerate spine curves in this model are rough estimates based on range of motion and stiffness of the neutral zone data reported by other studies. Full force deflection curves for levels of degeneration are not available [7]. The literature review in Chapter 2 shows a lack of data which accurately and fully determines the effects degeneration has on the spine, and proposes a study be done to acquire the necessary data.

The functional spinal unit (FSU) is the smallest physiological motion unit of the spine. It consists of two vertebrae and the disc between them, along with all tendons and muscle tissue connecting them. Every FSU within the spine has a unique geometry, and every individual has a unique spine; the force-deflection curves for every spinal segment may vary widely depending on the differing geometries of the FSU [8, 9].

To accommodate the largest group of people, multiple versions of the spinal device could be made using different geometries, with every different version having incorporated into its design alterability so that it can be adjusted for individuals within the range of the device. It is anticipated that there may be therapeutic benefits to intentionally adjusting the device's stiffness according to changes in the surrounding tissue structure. Additionally, due to the non-linear nature of the natural force deflection curve of the spine, and due to this non-linearity providing passive stabilization to the spine, a non-linear force deflection curve is a desirable function for the device. The device needs to be small enough to fit between pedicles without interfering with the surrounding body mechanics. It was proposed by a surgeon advisory board that this space should be no wider than the pedicle screw heads and no longer then the screws are apart, which would be approximately 12 x 12 x 15 mm.

The following chapter is a literature review of research that studied the effect of degeneration on the torque rotation curve of an FSU as well as a review of current spinal implant technology to establish functional requirements used in the design of the FlexSuRe™. Chapter 3 describes the design of a spinal implant with customizable and nonlinear stiffness. Chapter 4 discusses the modeling and bench-top testing of the implant, while Chapter 5 includes results from cadaveric testing. Chapter 6 describes research in decreasing implant size. Conclusions and recommendations are included in Chapter 7.

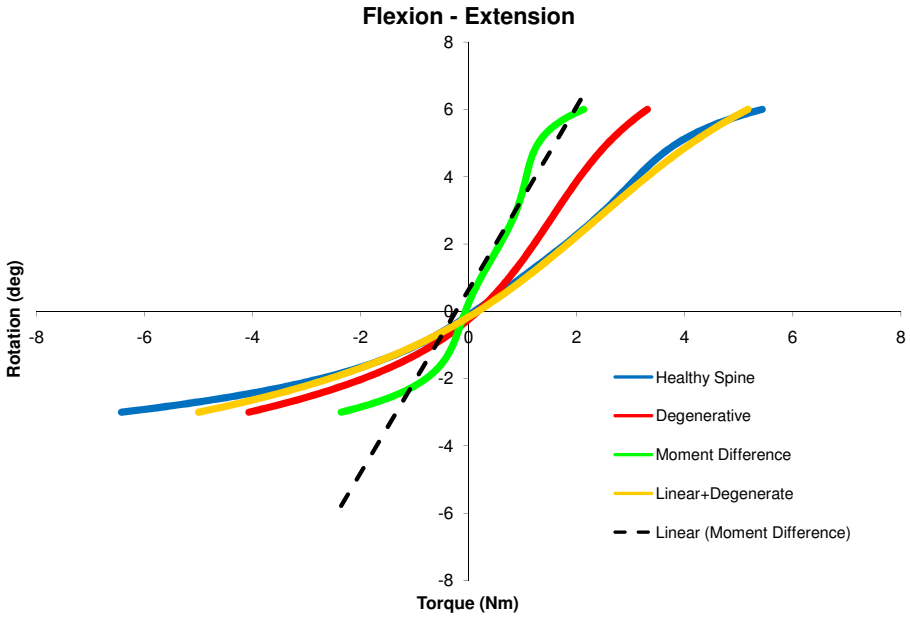

Figure 1.2: Restoring the degenerative spine to a healthy position. Figure from Stratton 2010 [6]

CHAPTER 2. EFFECTS OF DEGENERATION ON THE TORQUE ROTATION CURVE OF A FUNCTIONAL SPINAL UNIT

This chapter establishes design requirements for the development of a posterior dynamic re-stabilization system which can restore a compromised FSU to healthy kinematics and kinetics. Joint mechanics of the intervertebral disc are very complex, moreover this joint works in conjunction with two facet joints and multiple interspinous ligaments and muscles which further complexify the biomechanical response of the system. Current literature is reviewed to establish techniques and adopted criteria from similar devices to establish these design requirements. The chapter also establishes the need of a study which determines the effect of disc degeneration on the FSU based on full force-deflection characteristics. Spinal disc degeneration is a process that naturally occurs as an individual ages. It has been shown that increased joint laxity is a symptom of disc aging and degeneration. [10] It has also been shown that disc degeneration is possibly accelerated by abnormal loading conditions, such as overloading or immobilization. [11] It was proposed that if the torque rotation curve of a degenerate spine could be obtained it could be compared to the non-degenerate curve and possibly corrected through mechanical means. One purpose of this literature review was to determine if a study has been done to quantify the degenerate torque rotation curve. Recent studies have shown that testing the spine under certain criteria generates data as close to in-vivo physiologic responses as possible. This study therefore searches for and rates documents relating to the topic at hand and this specific criteria.

2.1 Design Requirements

The design requirements for the compliant mechanism dynamic stabilization system were complex, but not unique. A study of current research was used to establish these design requirements and associated definitions.

Implant rejection must be avoided, therefore the use of materials that have previously been proven in joint arthroplasty and spinal implant applications is the safest approach to the development of an implantable device [12].

Wear is an important factor in designing implantable devices. The majority of device failures in arthroplasty devices has been due to complications caused by wear and the resulting particulates. However, compliant mechanism design principles should guide the design to eliminate traditional wear-producing joints wherever possible [13–18].

Fatigue is another important aspect to consider during the device development. This device will be located in a position where it will experience fully reversed loading conditions as well as abnormal loading conditions. The device should last longer than the patient under the anticipated utilization loads. If a person were to be extremely active and put the device through a fully reversed load every 20 minutes during a normal 16 hour day for 40 years, this would result in 700,000 cycles during the lifetime of the device. If an individual needs such a device their activity level would be far less than this, therefore a target of one million cycles will suffice.

One primary use of posterior dynamic stabilization devices is to distract the disc space thereby relieving disc pressure. This distraction is intended to alleviate pain from pinched nerves as well as help with disc recovery. Therefore, the device must share compressive loads of up to 1200 N with the degenerated spinal segment. The load sharing ratio target is 30% load transfer to the device (up to 400 N) [11, 19, 20].

The device will be a posteriorly implanted, pedicle-screw attached device that fits within the established volume that surgeons currently use for posterior spinal fusion systems. Therefore the device needs to be as small as possible. A surgeon advisory board proposed that it should be no larger than the space directly between the pedicle screw constructs. This would leave a space of approximately 12 x12 x 15 mm. Additionally, the device needs to be smooth and not possess location in which tissue can be caught or damaged.

It is important that the spinal segment is returned to a healthy motion pattern, deviation from healthy motion can cause adjacent level degeneration [21, 22]. Therefore the device must work with the existing spinal structures to restore a healthy motion pattern (helical axes and range of motion) to the degenerated spinal segment [23, 24]. It also needs to maintain a healthy amount of interpedicular travel [25, 26], as well as restore a healthy torque-rotation behavior to the spinal

segment in all modes of loading [27,28]. Section 2.2 discusses more fully the currently documented understanding of spinal kinetics and kinematics and the need for a more detailed study regarding the kinetics of the FSU.

Due to this device being a pedicle-screw mounted system, it is important to limit the moment induced on the pedicle screw which would result in loosening of the screw from the bone. The insertion load has been measured by previous studies and showed that the average was approximated to be 0.4 Nm [29, 30]. If the device is to avoid screw loosening it should stay below this insertion load.

Due to the variability inherent in biological structures it is favorable to develop a device that is capable of encompassing this variability. Moreover, there is a possibility for conditions with the patient to change and require adjustment of the device while in vivo. Therefore, the stiffness of the device in each mode of loading must be tailorable within the window of physiologic variability. Additionally, it is preferable if the device can be adjusted post op using a surgical procedure less invasive than the original installation surgery.

Lastly, the device must be manufactured using existing techniques that are common to the medical device field. Variations from these techniques would require development of new procedures and would result in much higher production costs. Table 2.1 sums up the design requirements established.

2.2 Establishing the Necessity of a Study Which Fully Defines the Effects of Degeneration

2.2.1 Necessary Criteria to be Met

It is necessary to understand how the torque rotation curve changes depending on levels of degeneration for each section of the spine. To accomplish this, testing must be performed in which the torque rotation curves for each spinal segment are looked at with respect to their individual levels of degeneration. Due to the nature of the data being collected the testing will need to be performed in-vitro, for this reason a follower load needs to be applied in order to allow the spine segment to act as close to in-vivo as possible. [31]

Table 2.1: Design requirements and definitions

Design Requirement	Description
Biocompatibility	Use materials that have previously been proven in joint arthroplasty and spinal implant applications.
Minimal wear	Material dependent limit on wear rate, however compliant mechanism design principles should guide the design to eliminate traditional wear-producing joints wherever possible.
Infinite fatigue life	The device should last longer than the patient under the anticipated loads.
Share compressive loads with the spinal segment	The device must share compressive loads of up to 1200 N with the degenerated spinal segment. The load sharing ratio target is 30% load transfer to the device (up to 400 N).
Surgical placement	The device will be a posteriorly implanted, pedicle-screw-attached device that fits within the space currently used for posterior spinal fusion systems. The should not possess location in which tissue can be caught or damaged.
Restore healthy spinal kinematics	The device must work with the existing spinal structures to restore a healthy motion pattern (helical axes and range of motion) to the degenerated spinal segment. It also needs to maintain a healthy amount of interpedicular travel.
Duplicate healthy spinal kinetics	The device must work with the existing spinal structures to restore a healthy torque-rotation behavior to the spinal segment in all modes of loading.
No pedicle screw loosening	Limit the moment induced on the pedicle screw which would result in loosening of the screw from the bone, approximately 0.4 Nm.
Tailorable	The stiffness of the device in each mode of loading must be tailorable within the window of physiologic variability.
Manufacturability	The device must be manufactured using techniques that are common to the medical device field.

Torque Rotation Curves for the Individual Segments

In order to design the device appropriately the entire torque rotation curve needs to be charted and not just the end points. One of the most important portions of the curve is the slope at the origin. Range of motion (ROM) is not a sufficient criteria due to the fact that it neglects the nature of the curve between the end points. It has been shown that as discs degenerate they become less stiff. [32, 33] This will cause the slope at the origin to increase. In order to bring the curve back to the non-degenerate case this slope must be accounted for. [6] It is also necessary to have not only the combined data in order to perform statistical analysis but the individual test as loads are applied. The test needs to be performed in such a manner that the load is applied as a pure moment, and the data for the torque applied as well as the motion of the segment are recorded simultaneously.

Grade of Degeneration for Each Spinal Segment

It is important to understand how each level of degeneration affects specific spinal segments. Each spinal segment is physiologically different and therefore will react differently under degenerate cases. By analyzing each section of the spine according to its level of degeneration a delta for each segment can be derived with a much smaller standard deviation.

Follower Load Applied

It was shown by Patwardhan et al. that by applying a follower load to the spine more physiologic loading conditions can be simulated. [31] By applying a compressive load using a follower load the spine will respond in a more natural way than without. It is desired that data be gathered as close to physiologic conditions as possible. Due to the likelihood that the torque rotation curve will be different while under physiologic compressive loads, data that did not use a follower load should not be considered.

2.2.2 Studies That Present Significant Data

The most significant articles relating to the current proposed study are, Tanaka et al. [33], Krismer et al. [32], Mimura et al. [10], and Fujiwara et al. [34]. All of these articles presented relationships between the motion of the lumbar spine and the levels of degeneration of those segments. All of these studies showed that with degeneration comes decreased stiffness. None of the articles however took into consideration all the necessary criteria for the proposed study.

Quality of Motion Studies

The article that most closely matches the sought after criteria was the study by Krismer et al. [33]. This study applied a moment to individual functional spinal units(FSU) and the data was analyzed in two pools of data, upper lumbar ranging from T12-L1 to L3-L4, and the lower lumbar ranging from L4-L5 and L5-S1. Every test was categorized by grade of degeneration using the Thomson's scale. The data was presented in tables including the standard deviation for axial rotation, lateral bending, flexion, and extension. Each individual FSU was potted separately,

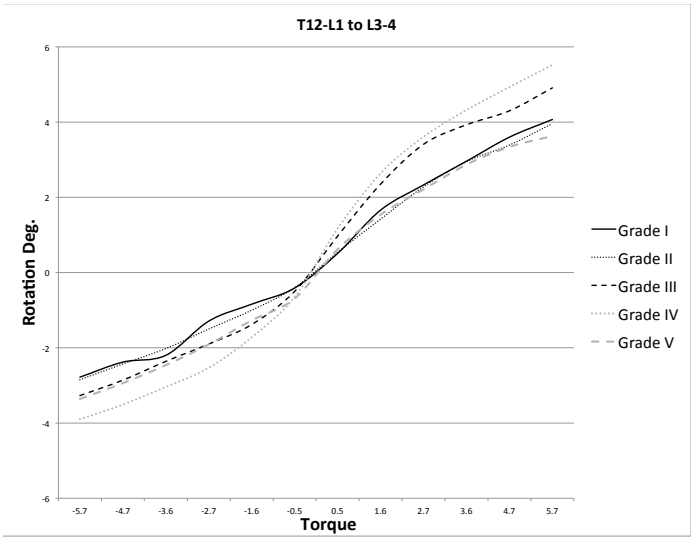

Figure 2.1: Torque rotation of the upper lumbar spine with grades of degeneration in flexion and extension. Data from Tanaka 2001 [33]

threaded rods were placed within the potting fixture such that there was a rod anteroposteriorly and transversely. Nylon balls were fixed to the potting fixtures for visual markers. Loads were applied by fixating a 530 mm moment arm to the threaded rods, and applying weights to the end of the moment arm. The weights used were incremented by 200 g starting at 300 g and going to 1100 g. The degree of rotation was calculated as well as the distance traveled in millimeters. There was no follower load applied. This study showed that the degree of rotation increased as degeneration increased up to grade 4 degeneration for the upper lumbar axial rotation and flexion. It also showed that for the upper lumbar lateral bending did not follow this trend but had less rotation for grade two and then more for grade 3 and back down for grades 4 and 5. Additionally it showed that for the lower lumbar there was no significant difference in the rotation as degeneration increased. From the data provided in the paper torque-rotation curves were created using the mean values for the flexion and extension tests. The charts for the upper lumbar and lower lumbar curves are given in figures 2.1 and 2.2.

This study showed how the spine does have a tendency to decrease in stiffness as degeneration occurs. This article however does not meet the above mentioned criteria. The data presented was not for the individual FSU, but for pools of FSU's within a range for the upper lumbar and lower lumbar portions of the spine. The data was collected without using a follower load, therefore

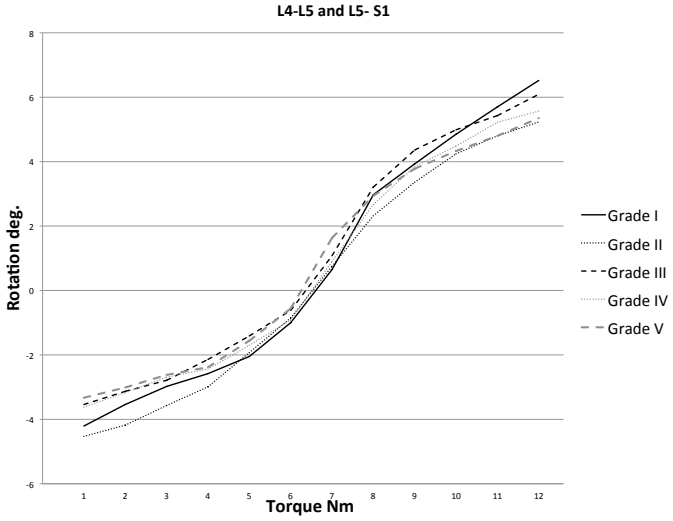

Figure 2.2: Torque rotation of the lower lumbar spine with grades of degeneration in flexion and extension. Data from Tanaka 2001 [33]

it is possible that the segments tested would have responded differently under more physiologic conditions. Additionally the loads were applied incrementally, it is not known how the loads were stepped up or how much time elapsed between each step. There are possibilities that the data has error due to stress relaxation of the soft tissue and creep. Moreover if the weight was taken off before the higher increment was applied hysteresis would have been neglected.

The next article that was highly significant was the article by Krismer et al. entitled "Motion in lumbar functional spine units during side bending and axial rotation moments depending on the degree of degeneration." This study performed tests on individual FSU for axial rotation of the lumbar spine. All segments of the lumbar spine given a specific level of degeneration were placed into the same pool of data for analysis. They classified the levels of degeneration according to the Nachemson, Thompson, Adams, and the Mimura degeneration criteria. The testing fixture was mounted on top of the potted FSU and a torque was applied using two pulleys creating a coupled load on the top vertebral body of the FSU. According to the diagram it appears that they performed testing on lateral bending using long moment arms and applied loads at the ends of the arms. This study however declared that their data for lateral bending was not significantly different between degenerate cases. This statement supports the findings of Tanaka et al. who did not find significant change due to degeneration in the lower lumbar spine in lateral bending or flexion and

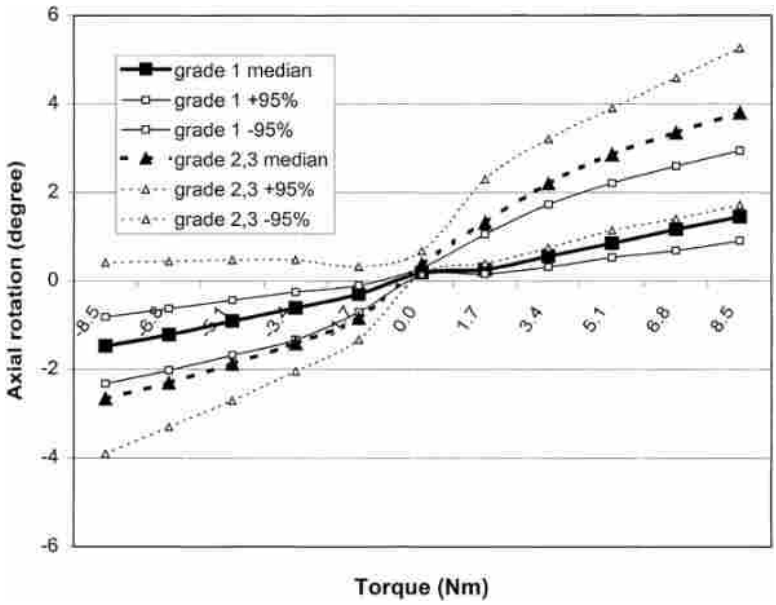

Figure 2.3: Torque rotation of the lumbar spine with grades of degeneration in axial rotation. Data from Krismer 2000 [32]

extension, they also agreed that the degrees of axial rotation was effected. A figure was provide which correlated the levels of degeneration to torque rotation in relation to axial rotation, their figure is provided in Figure 2.3. This graph does provide insight in that the curves act the way that was proposed. This study also does not meet the above criteria. It analyzes the spinal segments in an entire pool of one level of degeneration and is not level specific. The test fixture did not incorporate a follower load, and lastly they did not analyze flexion-extension nor did they present their findings for lateral-bending.

Range of Motion Studies

The next study of importance was by Mimura et al. titled "Disc degeneration affects the multidirectional flexibility of the lumbar spine." [10] They tested entire lumbar sections at a time. The degeneration in each disc was classified using a radiographic method and a microscopic method. They tested the spine by applying a pure moment to the top of the spinal unit using a specially designed headpiece. The headpiece produced pure moments using a system of opposing pneumatic actuators supported by linear bearings. This study documented and tested the multidirectional flexibility in terms of ROM, neutral zone and the neutral zone ratio. Using this criteria

they were able to show that degeneration was linked to the flexibility of the lumbar spine. They did this by showing that the Neutral zone ratio increased for all three loading conditions where degeneration was present. This study also does not meet the above criteria in that they did not test each vertebral segment separately, they did not provide any torque rotation curves, nor did they apply a follower load while applying the loads to the spinal section.

Fujiwara in the article "The effect of disc degeneration and facet joint osteoarthritis on the segmental flexibility of the lumbar spine" went a few steps further than Mimura et al. and looked at these degenerate conditions while taking into account osteoarthritis of the facet joint. This study analyzed each segment individually and classified them individually according to the Thompson's scale of degeneration. They also classified the level of degeneration of the facet joints according to a classification proposed by Grogan et al. [35] They tested the spine segments by potting them and then applying a pure moment using an unconstrained moment arm, the length of the arm is not specified, however up to 6.6 N-m were applied. From their findings they show that motion increased with degeneration. However, as degeneration progressed to stage five, motion significantly decreased. These findings support the findings of the previous articles with regards to the trends observed. One interesting point of information taken from Fujiwara is that motion increased with degeneration for both male and female however there was not significant change in the female for flexion extension or lateral bending. A figure from Fujiwara showing these trends is provided in Figure 2.4. Mimura also noted that there was a decrease in ROM in flexion and extension however the NZ increased, and they showed that this results in joint laxity. This study did not meet the above criteria due to not having information on individual segments, only providing ROM, and not applying a follower load.

Other Studies

Other studies which covered degeneration and mechanics of the lumbar spine included; J. Soini et al. [36], P. Kurkowski and A. Kubo [37], Christina A. Niosi and Thomas R. Oxland [38], An HS, Haughton VM, Lim T-H [39], Gertzbein SD, Seligman J, Holtby R, et al. [23], Kurowski P, Kubo A. [37], Umehara S, Tadano S, Abumi K, et al. [40], J. Seligman, S. Getzbein, M. Tile and A. Kapasouri [41], S. Campana et al. [42], Masashi Miyazaki et al. [24],and Jesse E. Bible et al. [43]. These articles provided great information on degeneration and motion correlations,

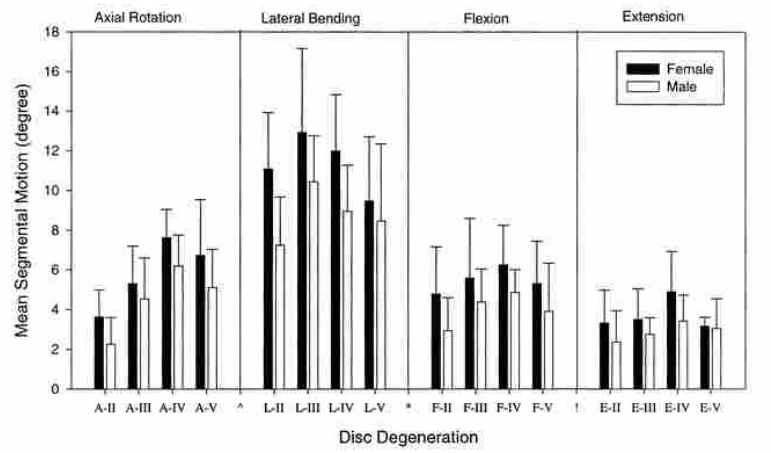

Figure 2.4: Effects of disc degeneration on segmental motion. Data from Fujiwara 2000 [34]

however were not as relevant as the previously mentioned articles. Many of these articles covered ROM, and some mostly covered loading conditions on the disk.

There were a few articles that were found which provided insight on degeneration however did not correlate that degeneration to the motion of the spine. These studies included; S Friberg and C Hirsch [44], H. Paajanen, M. Erkintalo, S. Dahlstrom, T. Kuusela, E. Svedstrom and M. Kormano [45] H.F. Farfan, R.M. Huberdeau and H.I. Dubow [46], and Klaus John Schnake, Michael Putzier, Norbert P. Haas, and Frank Kandziora [47].

Another area that provided insight and had some relevance involved instability of and injury to the vertebral disc. These studies were the following; Penning L, Wilmink JT, van Woerden HH. [48], Panjabi MM, Krag MH, Chung TQ. [49], W.H. Kirkaldy-Willis and H.F. Farfan [50], I.A.F. Stokes and J.W. Frymoyer [51], V.M. Haughton, T.A. Schmidt, K. Keele, and H.S. An and T.H. Lim [52].

The last catagory of studies that provided insight into the subject dealt with motion of the non-degenerate spine. The articles looked at included; Guan Y, Yoganandan N, Moore J, Pintar FA, Zhang J, Maiman DJ, Laud P. [53], Pennal GF, Con GS, McDonald G, Dale G, Garside H. [54], I. Yamamoto, M.M. Panjabi, T. Crisco and T. Oxland [55], A.B. Schultz, D.N. Warwick, M.H. Berkson et al. [56], Christoph Quack, Peter Schenk, Thomas Laeubli, Susanne Spillmann, Juerg Hodler, Beat A. Michel, and Andreas Klipstein [57], and Panjabi et al. [7].

CHAPTER 3. DESIGN OF A SPINAL IMPLANT WITH CUSTOMIZABLE AND NON-LINEAR STIFFNESS

3.1 Objective

The objective of this work was to build on the FlexSuRe™ spinal implant by adding the ability to modify the force-deflection curve produced to tailor the device to individual needs, and provide a non-linear force deflection profile that resembles the spine's force-deflection profile.

3.2 Methods

The goal of this work was the development of a device that would attach to two vertebral bodies, provide support and stability to the Functional Spinal Unit (FSU), and have the ability to be altered to provide variable stiffness characteristics. The device should be capable of spanning multiple FSUs using multiple devices in series. The device is comprised of compliant and rigid segments that provide a stiffness profile limiting all six degrees of freedom. Some degrees of freedom would be nearly completely constrained while only partially restricting others. The device stiffness can be made either linear or non-linear, depending on how various design parameters are used. The links comprising the device would be compliant, rigid, or a combination of both rigid and compliant segments. The joints between each link could be fixed, a cam surface, or contact aided. The shape of each rigid and compliant segment can be rectangular, prismatic, circular, triangular, spherical, cylindrical, or any other three dimensional shape. Through the manipulation of the links and their interaction, multiple stiffness characteristics were to be attained.

The foundation upon which most concepts were derived originated from previous work in the design of the FlexSuRe™ . Figure 3.1 displays the current configuration of the FlexSure™ as it is attached to the L4-L5 FSU using pedicle screws. The pedicle screw assembly has a large cylindrical head which attaches to the screw as well as to the FlexSuRe™ post. The FlexSuRe™ is composed of two posts, two flexures, and one base. The two flexures form a C-shape with a middle

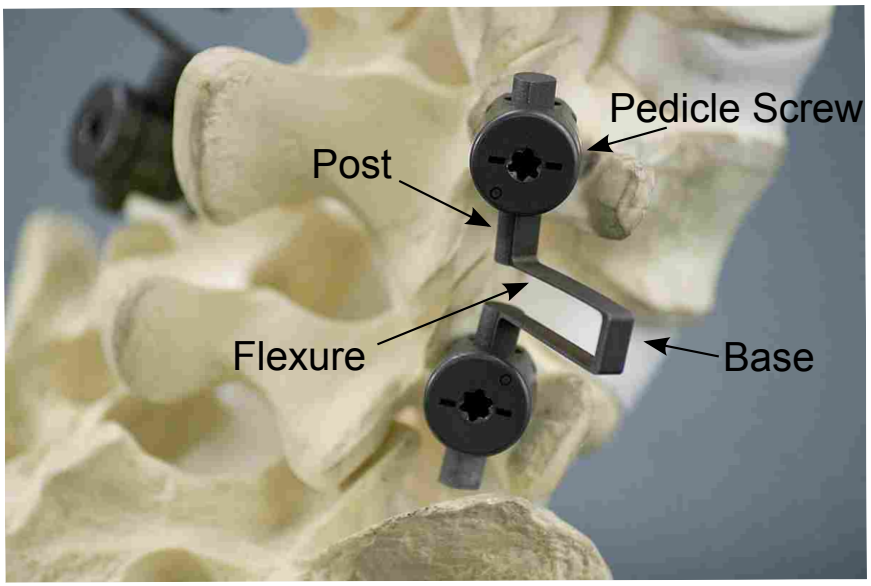

Figure 3.1: Prototype of the FlexSuRe™ with members labeled

base that is slightly thicker than the flexures. Components are positioned on either side of the two vertebral bodies to which they are attached. The resulting device is expected to have geometry similar to the FlexSuRe™ and the terminology of post, base and flexure is used in describing the design concepts presented within this work.

The customizable nature of the device can be achieved by a number of methods including: actuation of a built-in device to transform the flexures' geometry or position, the application of additional links (rigid, compliant, or compound), or by magnetically or electrically changing material properties. Using these methods the following alterations can be made: adjusting the lengths of the segments or links, pre-straining the device using axial compression or decompression and pre-torquing, changing the cross section of the members, adding or removing layers of same or different materials, altering the positional relationship of present links, providing a contact surface, as well as causing phase changes within the material using materials such as nitinol or a magneto-rheological or electro-rheological material.

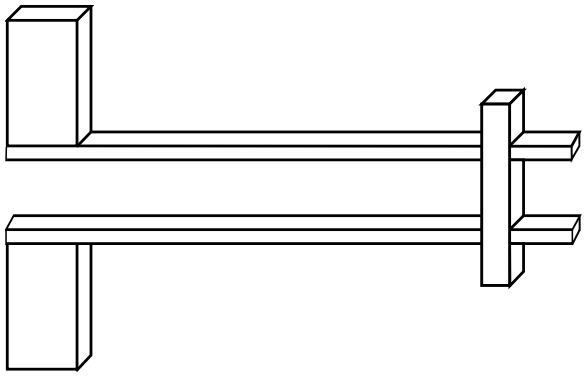

Figure 3.2: Customizable length using a base link attached by press fit

3.2.1 Concept Generation and Selection

Many device concepts have been explored and are presented in this document. The range of possible concepts are not limited to those presented here; however, they provide an example for various categories of designs.

Transforming the flexures' geometry, orientation or position was explored and some concepts identified can be found in Figures 3.2 and 3.3. These figures demonstrate concepts for elongating or shortening flexures. In Figure 3.2 the base link has been made rigid and is attached to the flexures by using a press-fit. The base links can be moved closer or farther from the post to change the flexure link length, and the press-fit will keep it from moving during actuation. Figure 3.3 goes further with this idea by adding an additional base link which has a lead screw attached. The base link with the lead screw controls the position of the press-fit base link. The lead screw is turned by a physician to achieve optimal positioning of the press-fit link, and to securely hold the moveable base link in place.

Figures 3.4, 3.5, and 3.6 demonstrate concepts for altering the device's force profile by incorporating pre-straining in the device. Figure 3.4 demonstrates using a spring and a screw for one base link and a rigid fulcrum for a secondary base link. The device is pre-strained by tightening the screw of one base link to decompress the other side. Figure 3.5 demonstrates preloading the ends of the flexures with a moment end load. This would be achieved by creating a post which has a customizable attachment point to the flexures. Figure 3.6 shows a concept for pre-torquing the ends of the flexures, or rotating the flexures using an adjusting screw and a set screw. The box containing the adjustment screw and set screw shown in Figure 3.6 would be attached to the post

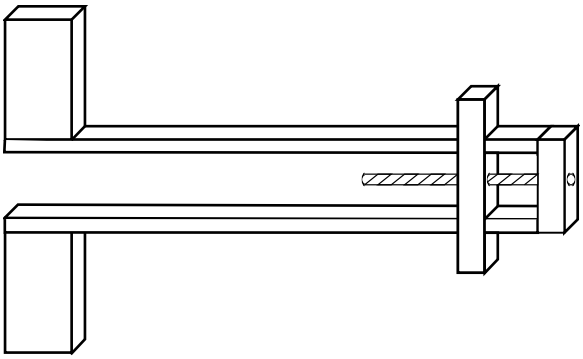

Figure 3.3: Customizable length using a screw

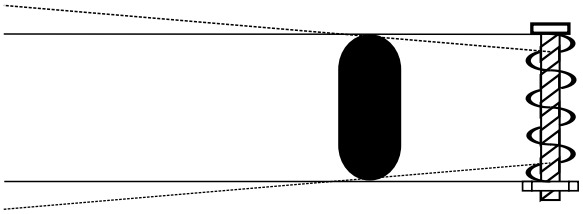

Figure 3.4: Pre-compressing using a screw

as well as the base links. If the adjustment screw was turned and set into place on the base side without adjusting the post side it would induce a pre-torque to the flexure. By adjusting both sides the orientation of the flexures would be rotated. The rotation of the link would cause different force deflection characteristics when the cross-sectional second moment of area is different for Ixx than for Iyy.

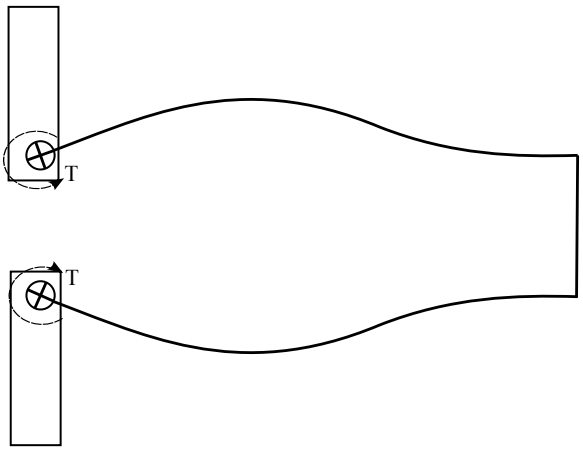

Figure 3.5: Pre-stressing using moment end loads

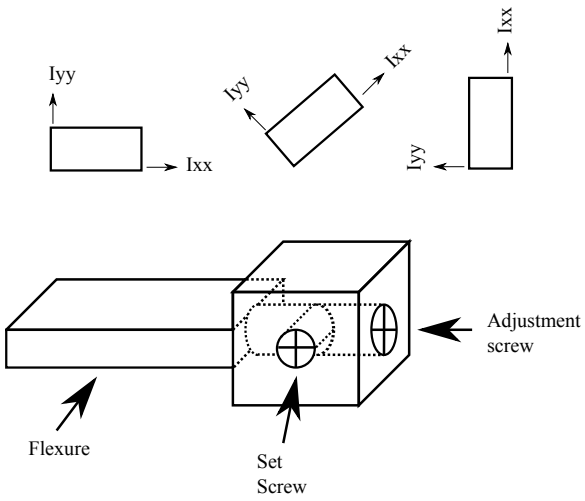

Figure 3.6: Pre-torquing using adjustment and set screws

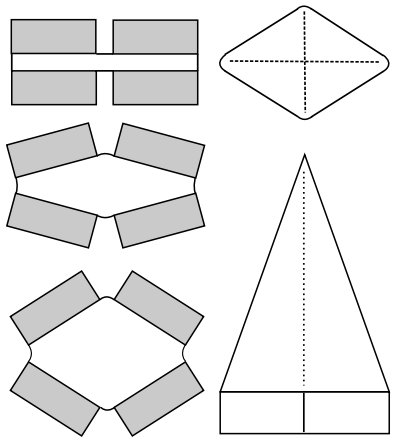

Figure 3.7: Variable cross-sectional area

Another example of changing the geometry was incorporated by changing the cross-sectional area of a flexure. Figure 3.7 demonstrates one concept for how this might be achieved by morphing a rectangular cross-section into a diamond shape. Four rigid segments are connected by four compliant living hinges (shaded elements on the left of Figure 3.7). Two of the diamond shaped cones (element on the right of Figure 3.7) are inserted into the sides of the beam, opening up the device and causing it to change from a rectangular shaped cross-secction to a diamond shape.

The concept of adding multiple links to the device is demonstrated by Figures 3.8, 3.9 and 3.10. Figure 3.8 demonstrates the concept of adding flexures using inserts. The base, flexures, and post of the initial device are one piece. The post has a hole in the middle allowing the insertable

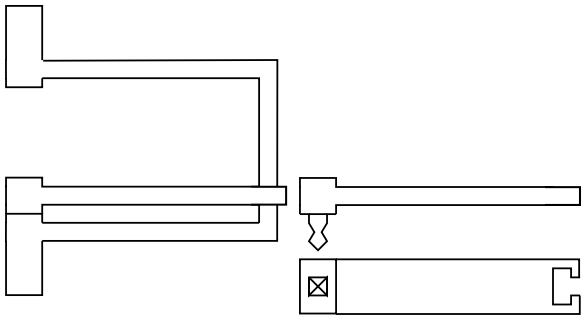

Figure 3.8: Adding multiple flexure design

flexures to snap into place. The base is slotted so that when the inserts are attached to it they cannot slide up nor down and therefore become rigidly attached. Figure 3.9 demonstrates how a flexure can be used so that it is only active during predefined positions of actuation. This concept uses a hollow post, and an additional flexure with an arm-piece. The idea behind this concept is that when the posts are compressed toward each other there will be a point when the arm of the additional flexure comes into contact with the top of the cavity on the post. When this occurs the additional flexures will have to be deflected to achieve further motion. The same thing will occur if the posts are separated and the arm of the additional flexures comes into contact with the bottom of the cavity on the post. Figure 3.9 shows the deflected position and the original position interposed on top of each other. Figure 3.10 shows how to combine the concepts of multiple flexures and variable length flexures. This device uses a base piece which has a vertical compliant link between two rigid end connectors. The end connectors are able to clamp down on the horizontal flexures at different locations along their length. The end connectors are also able to connect to only one set of flexures or both at the same time.

Figure 3.11 demonstrates how a contact-aided flexure would interact with a circular contact profile. Figure 3.12 shows two additional contact surfaces: elliptical and polynomial. The contact surface would be attached to the base link so that as the flexures deflected, and the posts came closer together, the flexures would come into contact with the surface. The flexure would be forced to follow a different path, which would result in a different force-deflection relationship.

Multiple flexures with variable lengths (Figure 3.10) and the contact aided FlexSuRe™ (Figure 3.11) were the two concepts selected for further modeling. Potential range of variability and ease of application were the two selection criterion which set these concepts apart from the others.

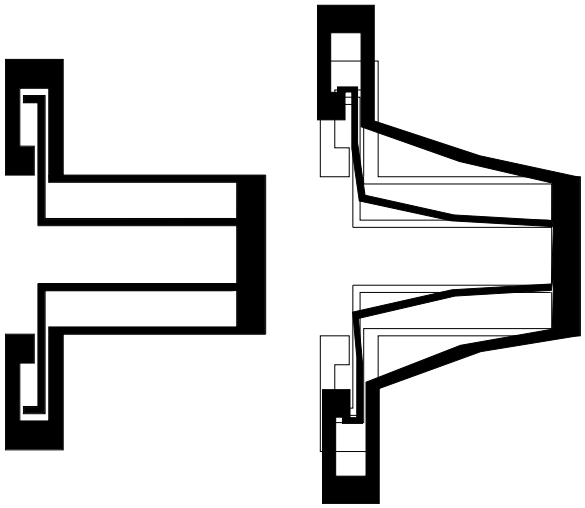

Figure 3.9: Adding flexures during actuation

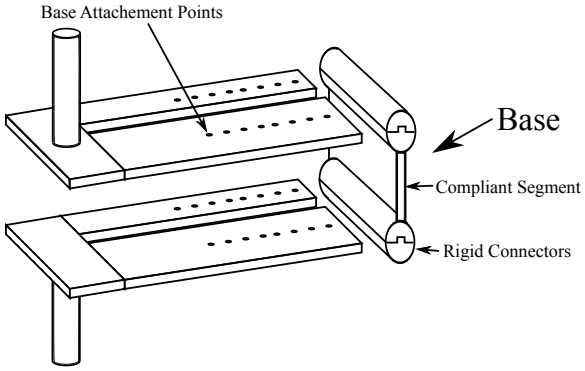

Figure 3.10: Multiple flexures with variable lengths

Mathematical models were used to define the potential range of variability for each concept given design parameters based on geometry restrictions and material properties of eligible materials. Ease of application was scored subjectively.

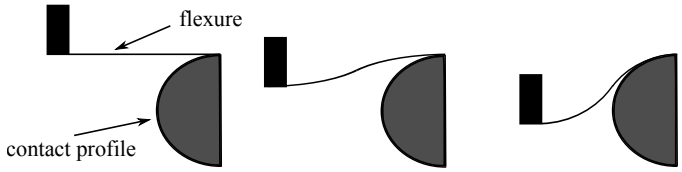

Figure 3.11: Contact-aided flexure shown deflected on a circular contact profile.

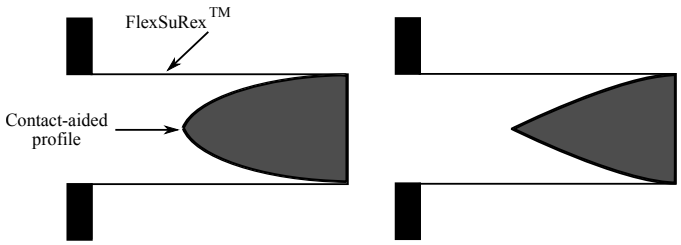

Figure 3.12: Contact-aided flexure and two different contact profiles

3.2.2 Modeling Top Concepts

Multiple flexures with variable lengths and the contact-aided flexure were the two concepts selected to be modeled in more depth. A program was developed to model the original FlexSuRe™ and provide force deflection characteristics of the device given geometric input. It was validated during the design phase of the original FlexSuRe™ [6]. The concept of multiple flexures with variable lengths was able to be modeled using the program by inputing various flexure lengths and widths. The material used in the modeling was Ti-6AL-4V and the material properties can be seen in Table 3.1. Exploration of the design space using the program resulted in a feasible geometry for a two-flexure, two-length FlexSuRe™ . This device would be able to have either or both flexures active at any given time, and the length can vary between 19 mm and 23 mm. Table 3.2 provides a sample of the data showing how this device would change force-deflection characteristics as more flexures were attached and as the lengths were changed. Increasing the thickness or decreasing the length increases the stiffness and reduces the rotation for a given torque. When both links are attached in parallel the rotation would be even less under the same load.

Table 3.1: Material properties used during modeling of concepts

Ti-6AL-4V

Property	Value
Youngs Modulus	113.8e9 Pa
Yeild Stress	880e6 Pa
Poisons Ratio	0.342

Table 3.2: Spinal segment rotation at input torques for various lengths and thicknesses

	Rotation (rad)					
	Thickness (5mm)		Thickness (10mm)		Combined Thickness (15mm)	
Torque (Nm)	Length (23mm)	Length (19mm)	Length (23mm)	Length (19mm)	Length (23mm)	Length (19mm)
-10	-4.32	-4.28	-4.22	-4.13	-4.13	-4.00
-2	-1.33	-1.24	-1.19	-1.07	-1.09	-0.96
2	1.64	1.54	1.49	1.35	1.38	1.20
10	7.79	7.61	7.54	7.17	7.29	6.74

The second concept, the contact-aided flexure, was modeled using a closed-form solution and a finite element model (FEA done in ANSYS see batch code in Appendix A). The closed-form solution used elliptic integrals and large-deflection beam theory. A Mathematica program was built to define the deflection of a flexure as it underwent a certain deflection and came into contact with a defined surface (see Appendix B). The program was capable of defining many different types of contact surfaces, and an elliptic surface was chosen for its changing radius of curvature. The output of the program provided the deflected beam shape as well as the force required to deflect a given amount. The device was modeled using the titanium alloy Ti-6AL-4V. The material properties are given in Table 3.1. The dimensions of the flexure are torsion length tl, torsion width tw, and thickness t. These dimensions as well as the elliptic surfaces semi-major and semi-minor axis a and b are shown in Figure 3.13 and given in Table 3.3, where a is defined relative to tl by a scaling factor of r_a.

Figure 3.14 shows multiple plots of the displacement profiles of the contact and non-contact-aided flexures as they undergo the same load steps. The solid line shows the contact-aided flexure, the dashed line shows the non-contact-aided flexure and the lightly dashed line shows the profile of the elliptical contact surface. The force-deflection relationship of the beam with and without the contact surface is shown in Figure 3.14. It was observed that the flexure alone produces a linear stiffness and the contact-aided flexure produces a non-linear stiffness profile. The curve fit equations of the lines, and the corresponding R^2 value for the non-contact and contact-aided

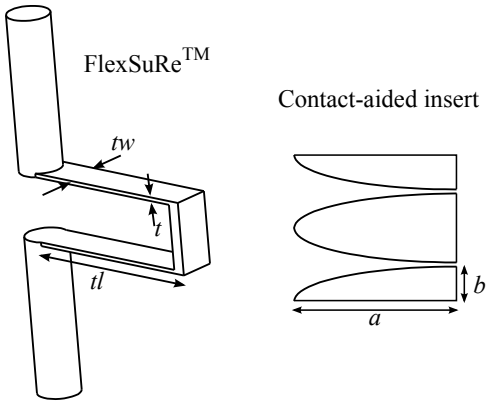

Figure 3.13: FlexSuRe™ and contact surface dimensions defined

Table 3.3: Flexure and contact surface dimensions

Dimension	Value (mm)
tl	21
tw	0.5
t	4
a	$r_a * tl$
b	3.75

flexures are

$$F = 0.0000157593 + 0.00013771\delta \tag{3.1}$$
$$R^2 = 0.999965$$

(3.2)

and

$$F = -0.0000555429 + 0.0001987763\delta \tag{3.3}$$
$$-0.0000105593\delta^2 + 2.25889 * 10 - 7\delta^3$$
$$R^2 = 0.999792$$

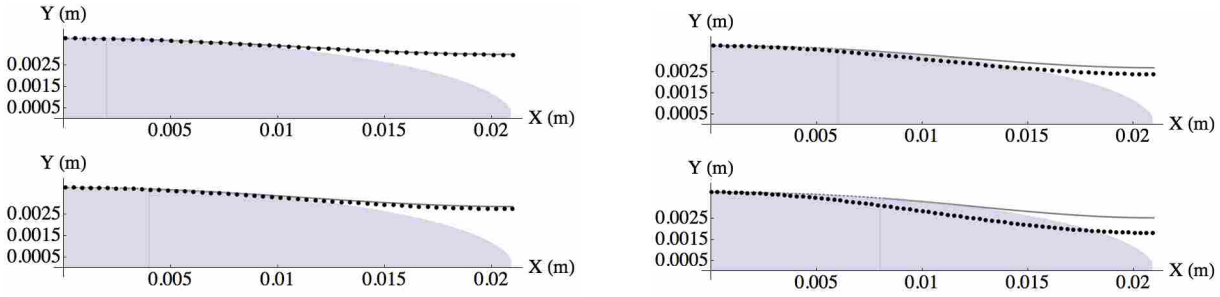

Figure 3.14: Displacement profiles of contact-aided and non-contact-aided flexures. The grey curve represents the contact-aided flexure(dotted where in contact), the black dotted curve is the non-contact-aided flexure.

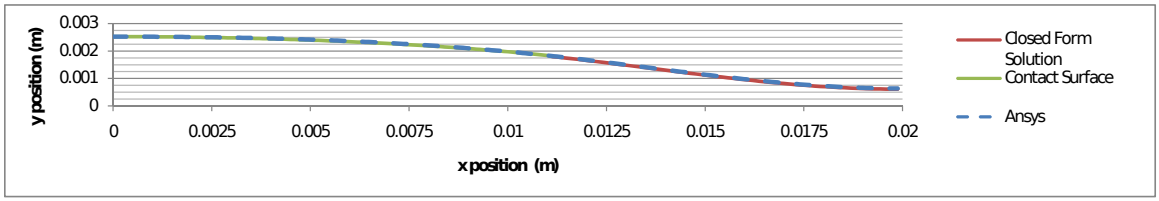

Figure 3.15: Displacement curves for closed form solution and ANSYS solution

where F is the reaction force produced for the given displacement of δ.

The device was also modeled using finite element analysis (FEA) for validation purposes. The results are compared to the closed-form solution for displacement and force deflection in Figures 3.15 and 3.16, respectively. The displacement graph in Figure 3.15 shows the closeness of the data of the closed-form solution to the FEA solution. The force-deflection curve displayed in Figure 3.16 verifies that using a contact-aided surface results in a non-linear force-deflection profile. The two concepts that were modeled both demonstrated feasibility and showed potential as implants. It was determined from the models that either concept would perform adequately, however the contact-aided device showed the greatest potential for the widest range of variability. It was decided to continue with the contact-aided design for the initial prototype and that the multiple flexures with varying lengths could be used in conjunction with the contact-aided design if additional variability was desired.

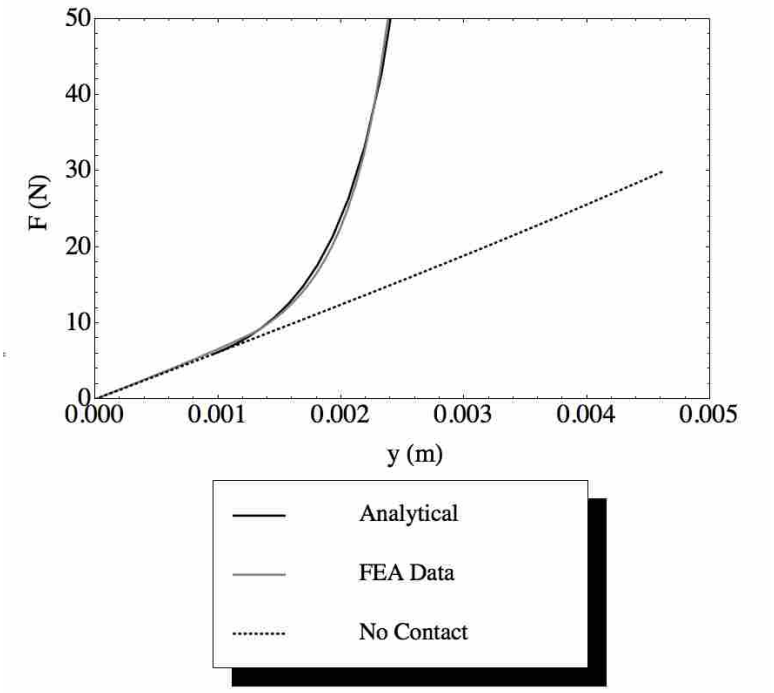

Figure 3.16: Force displacement profile for closed form non-contact-aided, contact-aided, and ANSYS contact aided models

3.2.3 Design and Geometry of Contact-Aided Attachment

From information gathered during modeling of the contact-aided flexure, a prototype was designed with an elliptical contact surface that attached to the original FlexSuRe™. The attachment design incorporates two parts which connect together and attach to the FlexSuRe™. Figure 3.17 displays the design for the concept prototype and displays how it attaches to the FlexSuRe™. The contact-aided attachment is designed to be wider than the flexures of the spinal implant, ensuring that there is no contact between the flexures and the back plate. Hard stops are designed which secure the spinal implant in the middle of the contact-aided attachment. The end plates covering the elliptic surfaces were designed to be large enough to cover the contact surfaces so that no tissue could get trapped between the flexures and the contact surface and become damaged.

The same elliptical curve was used for all four surfaces that come into contact with the flexures. The surfaces are positioned so that the flexures come into contact with them while decompressing or compressing. The elliptical curve used in conjunction with the flexures' geometry defines the stiffness of the implant. Differing elliptical curves would provide a wide range of

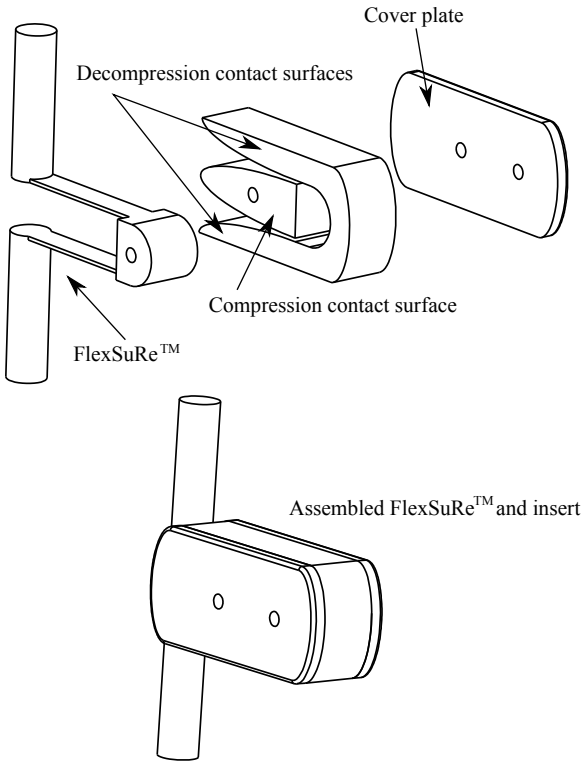

Figure 3.17: Contact-aided attachment for FlexSuRe™

variability. Additionally, different FlexSuRe™ geometries would provide additional variability. Surgeons will be able to approximate how stiff the device needs to be, and choose the best-suited FlexSuRe™ and then use the contact-aided devices to improve the fit. If after implantation it is determined that the implant needs to be stiffer of less stiff then the attachment can be replaced by a new attachment, thus allowing revision with minimal changes to the device.

CHAPTER 4. MODELING AND TESTING OF THE SPINAL IMPLANT

4.1 Introduction

The purpose of this paper is to introduce contact-aided inserts to be used with the FlexSuRe™ spinal implant and associated behavioral models that use elliptic contact surfaces that interact with the spinal implant to provide a nonlinear force-deflection curve and allow for customization of the device for individual force deflection need. The FlexSuRe™ spinal implant has the potential to provide stability after spinal surgery and facilitate the necessary mechanical support for possible regeneration of the spinal disc [6]. The spinal implant needs to restore the lost stiffness of a disc due to degeneration and also be tailorable for each person's needs to account for the difference in stiffness between a healthy disc and a degenerate disc. It is known that the spine exhibits a nonlinear force-deflection curve, therefore the inserts are designed to provide the spinal implant with a nonlinear curve that is tailorable to these needs. The spine is composed of multiple vertebra each separated by a cartilaginous disc, a functional spinal unit (FSU) is the smallest physiological motion unit of the spine, it consists of two vertebrae and the disc between them along with all tendons and muscle tissue connecting them. Every FSU within the spine has a unique geometry, and every individual has a unique spine; the force-deflection curves for every spinal segment may vary widely depending on the differing geometries of the FSU [8, 9]. Thus the inserts were designed to alter the spinal implant for specific individual needs.

The original design of the FlexSuRe™ can be seen attached to a FSU in Figure 1.1. The FlexSuRe™ is a compliant mechanism [58] that implements a variation of lamina emergent torsion joints [59]. This device is attached to the FSU using pedicle screws. The pedicle screw assembly has a large cylindrical head which attaches to the screw as well as to the post of the FlexSuRe™ . The FlexSuRe™ is composed of two posts, two flexures and one base. The two flexures and base form a C shape with the middle base thicker than the two flexures. Two flexures are positioned on either side of the two vertebral bodies to which they are attached.

The embodiment of the FlexSuRe™ shown in Figure 1.1 has a linear stiffness in the primary modes of loading (flexion, extension, axial torsion, lateral bending). This paper proposes using inserts to provide contact-aided deflections that result in the desired nonlinear stiffness. Contact-aided flexures can facilitate the creation of desired motions [60–63] and have been used for varied applications [64–66], including spinal implants [67]. Inserts with different geometries can be used to customize the implant performance for individual needs.

4.2 Models

An analytical model and a finite element model were used to verify the functionality of the contact-aided attachment (see Appendices A and B) . These models were compared to each other and then used to define a contact surface to be built and tested. The analytical model was derived by analyzing a beam in two sections, one portion in contact with a known surface geometry and the other portion a cantilever beam with known end conditions. The finite element analysis was performed using ANSYS and the contact surface tool was used while a series of beam elements were constrained to deflect in a fixed-guided motion.

4.2.1 Analytical Model

The analytical model was derived using beam theory and elliptical integrals. Due to the symmetry of the device, the analytical model was simplified to include only the unique portion of the geometry. An assumption of constant contact was made to analyze the contact portion of the beam. This assumption made it possible to know the conditions of the beam wherever it was in contact with the surface. An elliptic curve was used to demonstrate the contact-aided design, and elliptical integrals were used to evaluate the force-deflection curve of the free end of the beam using the values acquired from the contact surface portion and the known boundary conditions of the fixed-guided end.

Model for contact portion of the beam

Figure 4.1 shows the elliptical surface (the grayed area) and the beam which is represented by two segments: a dotted line where the beam is in contact with the surface and a solid line where

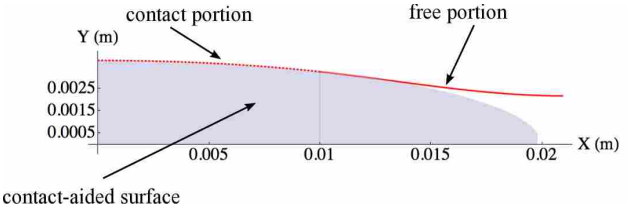

Figure 4.1: Interaction of the flexures of the FlexSuRe™ with the contact surface of the insert provides a tailorable nonlinear force-deflection response. The flexure was sectioned into two parts for analysis, one part in contact (dashed) and one part free of contact (solid).

the beam is free of contact. The equation of an ellipse in Cartesian coordinants x and y such that the model is defined to have the center of the ellipse at $(0,0)$ is

$$y = \pm \frac{\sqrt{a^2 b^2 (a^2 - x^2)}}{a^2} \tag{4.1}$$

where a and b are the semi-major and semi-minor axis of the ellipse.

With the contact surface defined, it is possible to calculate the portion of the beam that is in contact with the surface by integrating the arc length of the curve from $x = 0$ to the point where the beam leaves the contact surface. The infinitesimally small section of the curve, ds is

$$ds^2 = dx^2 + dy^2 \tag{4.2}$$

which can also be written as

$$\int ds = \int_0^c \sqrt{(1 + (\frac{dy}{dx})^2)} dx \tag{4.3}$$

The left side of the equation is integrated resulting in s or the length of the segment in question, the right hand side is integrated from 0 to c, which is where the beam leaves the contact surface. The arc length of the ellipse is

$$s = \frac{a\sqrt{1 - \frac{c^2}{a^2}} \sqrt{\frac{a^4 - a^2c^2 + b^2c^2}{a^4 - a^2c^2}} \mathrm{E}\left(\sin^{-1}\left(\frac{c}{a}\right), 1 - \frac{b^2}{a^2}\right)}{\sqrt{1 - \frac{c^2}{a^2} + \frac{b^2c^2}{a^4}}} \tag{4.4}$$

where $E(\phi, m)$ is the incomplete elliptic integral of the second kind. The length of the free end of the beam L can be calculated from

$$L = L_t - s \tag{4.5}$$

where L_t is the total length of the beam and s is the length of the beam in contact with the surface. The angle of the beam when it leaves contact with the elliptic surface is

$$\theta = \text{Tan}^{-1}\left(\frac{dy}{dx}\right) \tag{4.6}$$

Taking the derivative of y in Equation 4.1 with respect to x yields

$$\theta = -\text{ArcTan}\left(\frac{b^2 x}{\sqrt{a^2 b^2 (a^2 - x^2)}}\right) \tag{4.7}$$

The internal moment of a beam is assumed to be proportional to the beam's curvature, as in

$$M = EI\frac{d\theta}{ds} \tag{4.8}$$

where $d\theta/ds$ is rate of change of the angular deflection along the curve, E is Young's modulus and I the beam moment of inertia. The curvature $\mathrm{d}\theta/\mathrm{ds}$ can be rewritten using cartesian coordinates y and x [58] and

$$M = EI\frac{d^2 y}{\mathrm{dx}^2}\left(1 - \left(\frac{\mathrm{dy}}{\mathrm{dx}}\right)^2\right)^{-3/2} \tag{4.9}$$

The equation can then be evaluated using Equation 4.1 resulting in

$$M = -\frac{a^4 b^2 EI}{\sqrt{a^2 b^2 (a^2 - x^2)}\,(a^4 - a^2 x^2)\left(\frac{a^4 - a^2 x^2 + b^2 x^2}{a^4 - a^2 x^2}\right)^{3/2}} \tag{4.10}$$

Model for free section of the beam

Knowing the position (y, x), length (L), angle (θ) and moment (M) of the beam where it leaves the contact surface, it is possible to solve for the reactions in the remainder of the beam not in contact. Shoup and McLarnan developed equations for a beam loaded with vertical, horizontal,

and moment end loads [68]. The equations are

$$\begin{aligned} 0 = &\left(2k^2 \sin(\phi_1)^2 - 1\right) \sqrt{P^2 + Q^2} \\ &+ P\cos(\alpha_1) + Q\sin(\alpha_1) \end{aligned} \tag{4.11}$$

$$\begin{aligned} 0 = &\left(2k^2 \sin(\phi_2)^2 - 1\right) \sqrt{P^2 + Q^2} \\ &+ P\cos(\alpha_2) + Q\sin(\alpha_2) \end{aligned} \tag{4.12}$$

$$M_1 = 2k\sqrt{EI}\left(P^2 + Q^2\right)^{1/4} \cos(\phi_1) \tag{4.13}$$

$$M_2 = 2k\sqrt{EI}\left(P^2 + Q^2\right)^{1/4} \cos(\phi_2) \tag{4.14}$$

$$0 = -\frac{L(P^2 + Q^2)^{1/4}}{\sqrt{EI}} + F(\phi_2, k^2) - F(\phi_1, k^2) \tag{4.15}$$

$$\begin{aligned} 0 = &-\frac{H(P^2 + Q^2)^{3/4}}{\sqrt{EI}} \\ &+ Q\Big(2E(\phi_2, k^2) - 2E(\phi_1, k^2) \\ &- F(\phi_2, k^2) + F(\phi_1, k^2)\Big) \\ &+ 2kP\Big(\cos(\phi_1) - \cos(\phi_2)\Big) \end{aligned} \tag{4.16}$$

$$\begin{aligned} 0 = &-\frac{W(P^2 + Q^2)^{3/4}}{\sqrt{EI}} \\ &+ P\Big(2E(\phi_2, k^2) - 2E(\phi_1, k^2) \\ &- F(\phi_2, k^2) + F(\phi_1, k^2)\Big) \\ &+ 2kQ\Big(\cos(\phi_1) - \cos(\phi_2)\Big) \end{aligned} \tag{4.17}$$

There are seven equations which contain thirteen components, requiring six components to be known to solve for the remaining seven. Ten of the components are defined in Figure 4.2. They are horizontal force P, vertical force Q, moment end loads M_1 and M_2, end coordinates of the beam W and H, the length of the beam L, Youngs modulus and the beam moment of inertia combined EI, and the end angles of the beam α_1 and α_2. The angular deflection along the beam θ is shown and is evaluated using the limits of integration ϕ_1 and ϕ_2. The variable k is the modulus for the elliptic integrals. Equation 4.5 provides the value for the free beam length L. The angle α_2 is defined by evaluating Equation 4.7 and the end moment M_2 is acquired from evaluating Equation 4.10. The other three needed values are acquired from the known end conditions and physical properties of the beam. EI are known physical properties, P is zero for the fixed-guided case where the beam is free to move in that direction. The constant $\alpha 1$ is also known to be zero. Therefore, the six known quantities are L, EI , α_2, α_1, M_2, and P. The values that are to be solved for are ϕ_1, ϕ_2, M_1, Q, k, H, and W. Substituting into Equations 4.11 to 4.15 results in

$$\phi_1 = \sin^{-1}\left[\frac{1}{\sqrt{2}k}\right] \tag{4.18}$$

$$\phi_2 = \pi - \sin^{-1}\left(\frac{\sqrt{1+\sin(\alpha_2)}}{\sqrt{2}k}\right) \tag{4.19}$$

$$M_1 = 2\sqrt{kEIQ}\cos(\phi_1) \tag{4.20}$$

$$Q = \frac{M_2^2}{4k^2 EI\cos(\phi_2)^2} \tag{4.21}$$

$$0 = -\frac{L(Q^2)^{1/4}}{\sqrt{EI}} + F(\phi_2, k^2) - F(\phi_1, k^2) \tag{4.22}$$

To solve for the curve of the elastic beam Equations 4.18 and 4.19 are evaluated using the known quantities and their values are used to evaluate Equations 4.20 and 4.21. Equation 4.22 is then evaluated using the values derived from the previous equations and the known quantities. The root of Equation 4.22 will be the value for k. Equations 4.16 and 4.17 are evaluated using the known

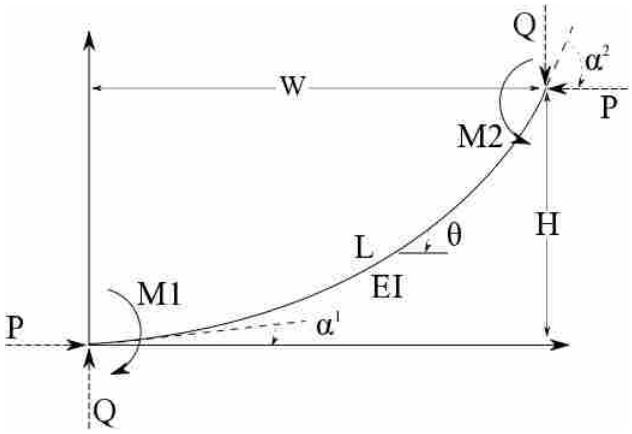

Figure 4.2: The general flexible beam

quantities resulting in

$$H(\phi) = -\frac{1}{Q^2}^{3/4}\sqrt{EI} + 2QE(\phi_1,k^2) - 2QE(\phi,k^2) - QF(\phi_1,k^2) + QF(\phi,k^2)\Big) \tag{4.23}$$

$$W(\phi) = -\frac{1}{Q^2}^{3/4}\sqrt{EI} \Big(2kQ\cos(\phi_1) - 2kQ\cos(\phi) \tag{4.24}$$

The values from Equations 4.18 to 4.22 are then used to evaluate Equations 4.23 and 4.24 where ϕ is evaluated from ϕ_1 to ϕ_2, the result is the position of the free section of the beam.

Results of Analytical model

The force-deflection profile of the contact-aided beam was defined by evaluating Equations 4.5, 4.7, 4.10, and 4.18 to 4.24 for increasing values of x (the horizontal point of liftoff from the contact surface). The elliptic contact surface was defined using

$$a = r_a L_t \tag{4.25}$$

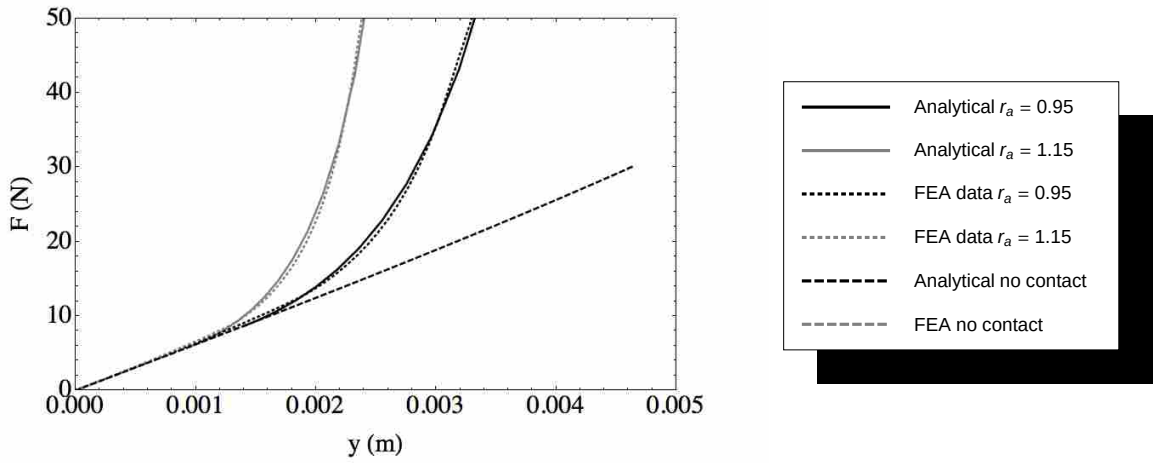

Figure 4.3: Force versus displacement curves for analytical and FEA data.

and

$$b = r_b L_t \tag{4.26}$$

where a and b are functions of the total beam length L_t where r_a and r_b are scaling constants. The values for Q (vertical force) and H (vertical displacement) at the end of the beam for every iteration of x was plotted in Figure 4.3. This plot shows the force deflection profile of the beam without a contact surface, and with contact surfaces for increasing values of the scaling constant r_a.

The force-deflection curve of a fixed-guided beam without a contact surface was acquired using Equations 4.11 - 4.17. The beam for this case was not divided into two segments and had end conditions of a fixed-guided beam, which are zero slope at each end $\alpha_1 = \alpha_2 = 0$, zero horizontal forces $P = 0$, with the total length of the beam $L = L_t$, and evaluating the equations given increasing values of Q. Using these six known quantities the remaining seven can be acquired.

Figure 4.3 illustrates that the contact surface provides a nonlinear force-deflection curve, and by changing the values for r_a (the scaling factor of the semi-major axis) the force-deflection profile can be altered. Stress verses displacement is plotted in Figure 4.4. These figures show how the device can get more force for the same deflection of the non-contact-aided beam.

4.2.2 Finite Element Model

The device was also modeled by finite element analysis (FEA) using ANSYS. The FEA model consisted of beam elements constrained to move in a fixed-guided motion while coming

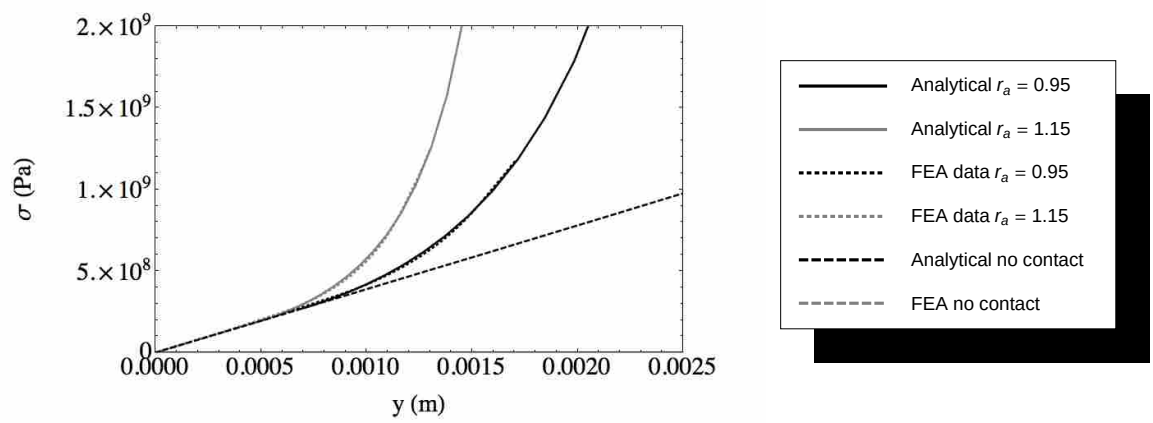

Figure 4.4: Stress versus displacement curves for analytical and FEA data.

into contact with an elliptically curved surface. The flexure was deflected in the y direction while free to move in the x direction and fixed from rotation at the ends. The model was evaluated such that the device was stepwise deflected in a static analysis and no dynamic effects were taken into account. Figure 4.5 shows the deflected position of the flexures given three different contact surfaces and how those deflections compared to the results from the analytical solution. In Figure 4.5, the dotted line is the solution from FEA and the solid line is predicted by the analytical model. The force-deflection curves from the FEA are compared with the analytical model in Figure 4.3, and the stress per applied force results from FEA are compared with the analytical model in Figure 4.4. As can be seen from these graphs, both models demonstrate comparable results.

It was observed in the FEA model that, during deflections past the height of an elliptical section, lift-off occurred. The assumption of constant contact used in the analytical solution is only valid for deflections equal to or less than the height of the semi-minor axis of the ellipse, b. The FlexSuRe™ was designed to deflect 2 mm and the smi-minor ais of the ellipse was 3.75 mm therefore constant contact which also includes no slip was achieved resulting in wear being negligible.

4.3 Physical Testing

Two designs were selected to be fabricated, tested, and compared to the models. Two elliptical surfaces were chosen with $r_a = 0.95$ and $r_a = 1.15$. Both surfaces had the same r_b value

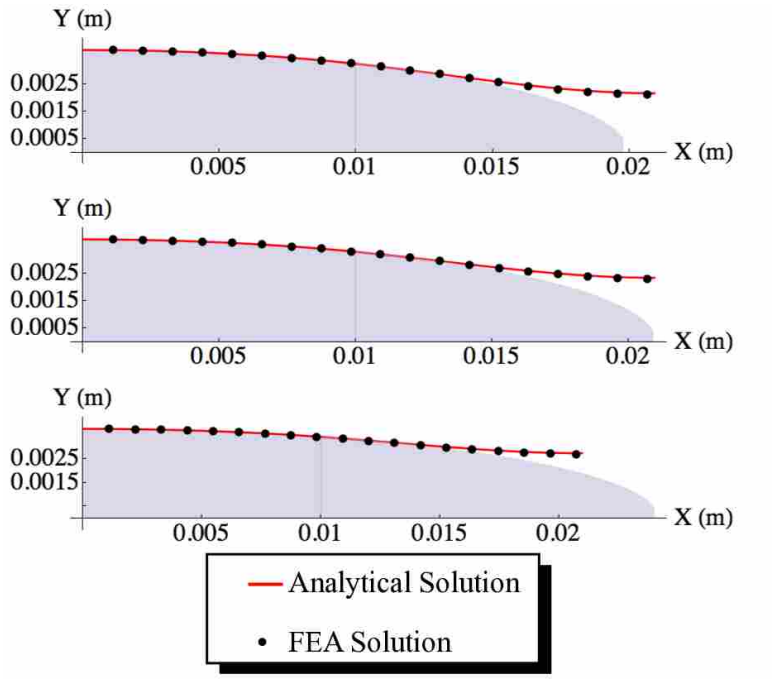

Figure 4.5: Comparison of displacements predicted by the analytical model with those predicted by FEA using ANSYS. The three curves are from top to bottom, $r_a = 0.95, r_a = 1.00, r_a = 1.15$.

of 0.1875. The prototypes were built and attached to the FlexSuRe™ and then tested on a tensile test machine and the results compared to the models.

4.3.1 Set Up

Figure 4.6 shows the FlexSuRe™ with the contact aided surfaces incorporated. A cover plate is used to enclose the device and is not shown in this figure. The FlexSuRe™ has symmetry about the horizontal axis. Therefore, the top and bottom flexures will act like springs in series. With an equivalent stiffness of

$$\frac{1}{K_F} = \frac{1}{K_t} + \frac{1}{K_b} \tag{4.27}$$

where K_F is the stiffness of the FlexSuRe™ , K_t is the stiffness of the top flexure and K_b is the stiffness of the bottom. Due to symmetry

$$K_t = K_b = K \tag{4.28}$$

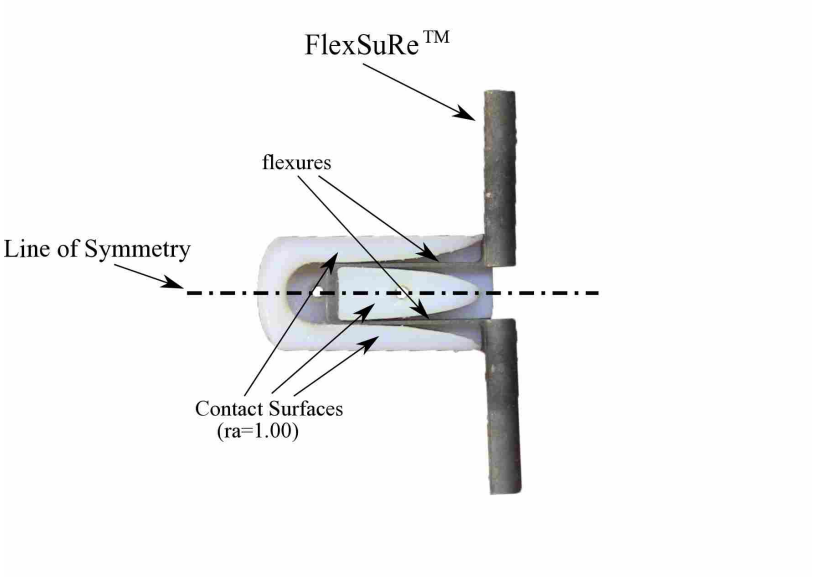

Figure 4.6: Prototype to be tested

and

$$K_F = \frac{K}{2} \tag{4.29}$$

The device was connected in series with a five pound load cell in a tensile test machine (Instron-model 1321). The device was tested in compression and extension with three different configurations: no contact surface, contact surface with $r_a = 0.95$, and contact surface with $r_a = 1.15$. The test was performed at a quasi static loading rate of 0.01 mm per second to eliminate dynamic effects and be comparable to the results of the models.

4.4 Discussion of Results

The experimental results are plotted with the analytical and FEA curves in Figure 4.7. The resulting curves follow the predicted trend of the analytical and FEA models. There is some discrepancy with the point at which the curve becomes nonlinear and the initial slope at that point. This was due to the fact that the prototype contact surface was not completely elliptic due to limitations in the fabrication process. The top of the ellipse was actually a flat section which transitioned into an ellipse and was not in contact during the initial portion of displacement. The models do not take into account that the beam was not in contact for the first 1 mm of displacement. This explains why the model data is slightly offset from the test data. Moreover there was a

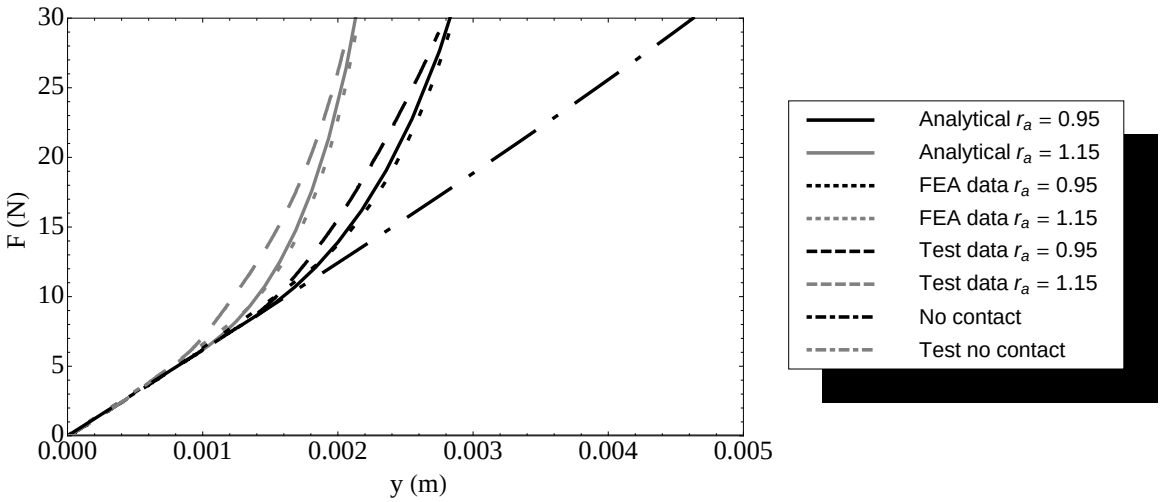

Figure 4.7: Test data collected for each surface compared to the analytical and FEA anticipated results.

transition from being in contact with the flat portion to being in contact with the elliptical section. This transition can be seen in the data and is most pronounced in the $r_a = 1.15$ plot. After the beam comes into contact with the ellipse, it follows the prescribed trend. Also, the models assume a perfectly rigid contact surface, which is not the case in the physical prototype. It was found that the assumption of no lift-off from the contact surface was untrue at deflections greater than b the semi-minor axis of the ellipse. However, the device was designed so that it would stay well away from this deflection and future designs will need to take this into account.

CHAPTER 5. CADAVERIC TESTING ON A CUSTOM-BUILT SPINE TESTER

5.1 Introduction

Cadaveric human lumbar spinal testing was used to explore the effects of attaching the FlexSuRe™ spinal implant with and without contact-aided inserts to a functional spinal unit (FSU). The contact-aided inserts provide an elliptic surface which contacts the compliant members of the FlexSuRe™ . These elliptic sections increase the device stiffness and produce a non-linear force-deflection curve. Two different inserts were used. The inserts are categorized based on the semi-major axis of the ellipse and the length of the flexures. The insert's semi-major axis length is a ratio of the flexure length, or r_a. The two inserts that were used had r_a values of 0.95 and 1.15.

5.2 Set Up and Procedure

A human lumbar cadaveric L4-L5 FSU was attached to a spine tester capable of loading the FSU with a pure moment load in flexion-extension, lateral-bending and axial-rotation. The spine tester also applies a follower load to simulate in-vivo loading conditions [31]. The tests were performed in an environmental chamber that kept the spinal segment at body temperature and near 100% humidity. The spinal segment was exercised in all three modes of loading to precondition the spine after thawing. Testing did not occur until preconditioning resulted in a repeatable force-deflection curve.

The FSU was then exercised in all three modes of loading while force-deflection data was recorded. Force was recorded using a torque transducer connected in series with the stepper motor that applied the moment load. The spines were tested at a loading rate of one degree per second. Deflection data was recorded using two cameras that recorded positional data for every recorded torque load. The rotational data was processed using in-house image tracking software. The rotational data was combined with the force data and plotted for every direction of loading.

Four tests were performed on the FSU for each mode of loading.

1. without any device attached (which in this study will be called the natural condition)
2. with the FlexSuRe™ attached
3. with the FlexSuRe™ attached and insert of $r_a = 0.95$
4. with the FlexSuRe™ attached and insert of $r_a = 1.15$

For every direction of loading, the four tests were performed without detaching the spinal segment from the machine or removing the compressive follower load, except between loading directions. The tests of flexion-extension, lateral-bending, and axial-rotation were randomly ordered, as was the sequence of the four test conditions. This was done to ward variance due to the order of testing.

After data was collected and processed to obtain force-deflection data, the data was curve fit using a dual inflection point Boltzman (DIP Boltzman) equation [69] BZ as follows,

$$BZ(T) = \frac{A}{1+e^{\alpha 1*(m-m1)}} - \frac{B}{1+e^{\alpha 2*(m-m2)}} + B; \tag{5.1}$$

This equation has been modified from the original Boltzman equation to include two inflection points; thus it has been termed the dual-inflection-point Boltzman equation. Each parameter has a specific meaning with regards to the curve. A and B are the limits on the y axis, where A is the rotation at maximum negative torque and B is the rotation at maximum positive torque, $m1$ and $m2$ are the moment values at the inflection points, $\alpha 1$ and $\alpha 2$ are related to the rate of change at the inflection points, and m is the applied moment. A and B were defined using the end points of the data and represent the range of motion (ROM) [53], and m is the independent variable. The other four parameters are fit to each curve of the data. The data contains two sets which are each fit with the DIP Boltzman equation due to hysteresis caused by physiologic conditions of the soft tissue. The two portion of the hysteresis will be called the upper and lower curves respectively. Figures 5.1, 5.2, and 5.3 show the raw data points as a scatter plot with the resulting DIP Boltzman curve fit overlaid.

To compare the results of the testing, the stiffness of each curve is defined and compared. The stiffness of the curves are defined by the ROM and the stiffness of the neutral zone (Knz)

which is defined by

$$Knz = \frac{m2 - m1}{\theta 2 - \theta 1} \tag{5.2}$$

where $\theta 1$ and $\theta 2$ correlate to their respective moment values $m1$ and $m2$.

5.3 Results

The FSU was tested in all three modes of loading and under the four specified conditions. The results for flexion-extension during the four test conditions are shown in Figure 5.1. The DIP Bolzman curve fit is also shown in Figure 5.1. The parameters that are changed to fit the data are $\alpha 1, m1, \alpha 2$, and $m2$. A table containing the values for each parameter for every flexion-extension plot is shown in Table 5.1 (note that the data has been fit for both the upper and lower hysteresis curves). This table also shows the R^2 fit and average variance of each curve for the values given.

Similar to the flexion-extension data, the results of lateral-bending for the four different tests are shown in Figure 5.2. The values for each parameter for lateral-bending plots are listed in Table 5.2.

The results of axial-rotation for the four different tests are shown in Figure 5.3. A list of values for each parameter for the axial-rotation plots are provided in Table 5.3.

The results of the four testing conditions were compared to evaluate how the FlexSuRe™ spinal implant and inserts affect the force-deflection behavior of the FSU. Figures 5.4, 5.5, and 5.6 super impose the fitted curves for each test condition. The change from the natural condition is shown in the plots and is listed numerically in Tables 5.4, 5.5, and 5.6. These tables show the ROM

Table 5.1: Fit values for flexion-extension data

Test	Curve	A	B	$\alpha 1$	$m1$	$\alpha 2$	$m2$	R^2	Variance
FE Natural	Upper	-7.31	7.31	1.61098	1.26888	0.477669	0.401117	0.907841	1.9014
FE Natural	Lower	-7.31	7.31	0.65452	1.82131	0.965572	2.34516	0.919799	1.75312
FE FlexSuRe	Upper	-6.295	6.295	0.459727	0.0831744	0.868651	2.16939	0.962924	0.562348
FE FlexSuRe	Lower	-6.295	6.295	0.747537	3.50868	0.649439	1.3385	0.958266	0.62399
FE $r_a = 0.95$	Upper	-4.85	4.85	0.48965	-0.573502	1.14747	1.37472	0.951278	0.466069
FE $r_a = 0.95$	Lower	-4.85	4.85	0.812556	2.29002	0.535844	1.51735	0.953674	0.4265
FE $r_a = 1.15$	Upper	-4.295	4.295	0.534619	-1.21952	1.15472	1.53757	0.956972	0.311257
FE $r_a = 1.15$	Lower	-4.295	4.295	0.81922	1.43525	0.526684	2.14203	0.953715	0.32698

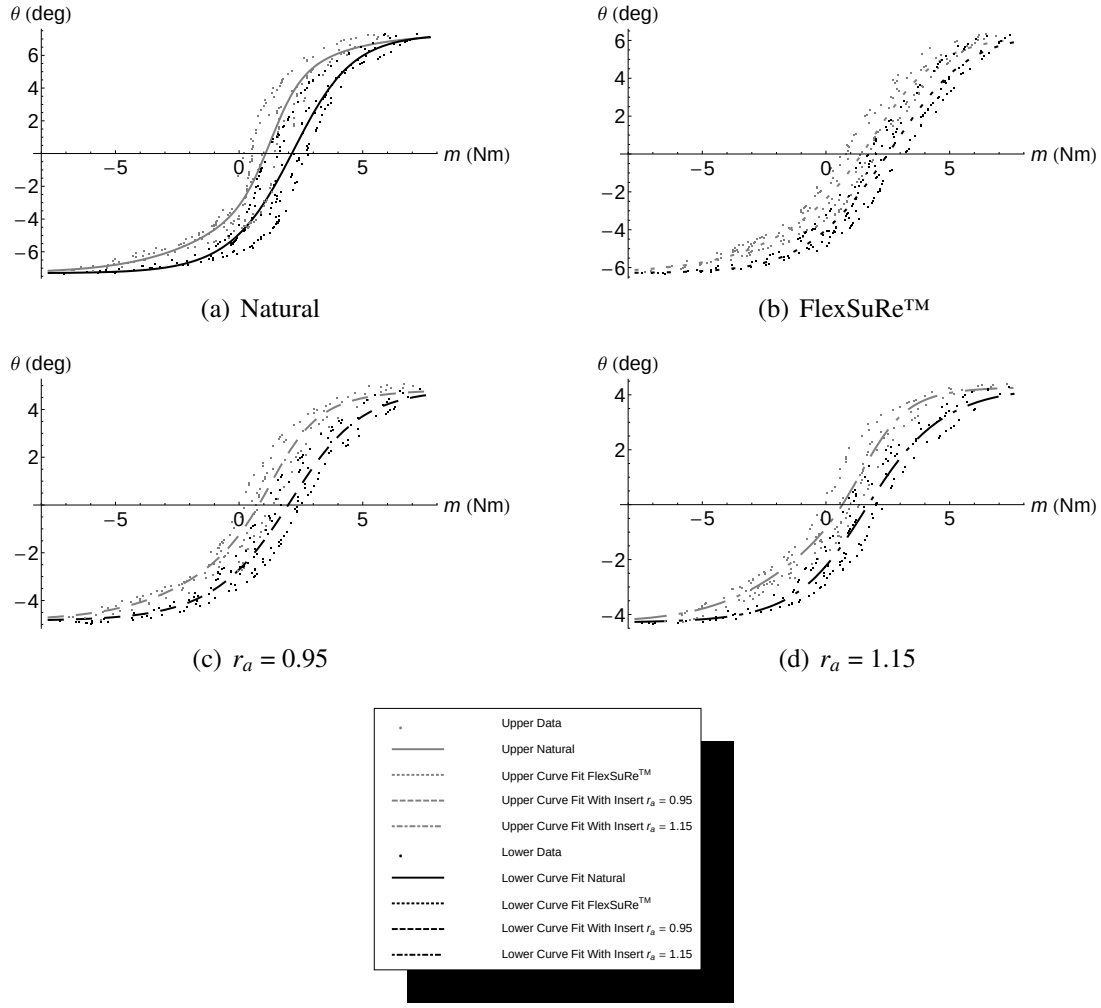

(a) Natural (b) FlexSuRe™

(c) $r_a = 0.95$ (d) $r_a = 1.15$

(e) Legend

Figure 5.1: Flexion-extension data and curve fit

Table 5.2: Fit values for lateral-bending data

Test	Curve	A	B	$\alpha 1$	$m1$	$\alpha 2$	$m2$	R^2	Variance
LB Natural	Upper	-11.06	11.06	0.599339	-1.95092	1.04862	-0.562361	0.932956	3.04072
LB Natural	Lower	-11.06	11.06	0.549755	1.73102	1.01109	0.0303975	0.930071	3.14312
LB FlexSuRe	Upper	-10.095	10.095	0.953081	0.285076	0.881507	-2.41405	0.911911	3.24697
LB FlexSuRe	Lower	-10.095	10.095	0.922446	-0.300509	0.68712	1.61142	0.926554	2.92548
LB $r_a = 0.95$	Upper	-9.965	9.965	0.955613	0.311724	0.884634	-2.46402	0.925479	2.79696
LB $r_a = 0.95$	Lower	-9.965	9.965	0.733635	0.125034	0.671784	1.25506	0.919218	2.92607
LB $r_a = 1.15$	Upper	-9.64	9.64	0.721748	-2.41113	1.116	0.0793287	0.917318	2.88009
LB $r_a = 1.15$	Lower	-9.64	9.64	0.635426	1.67618	0.903408	-0.153401	0.922829	2.60291

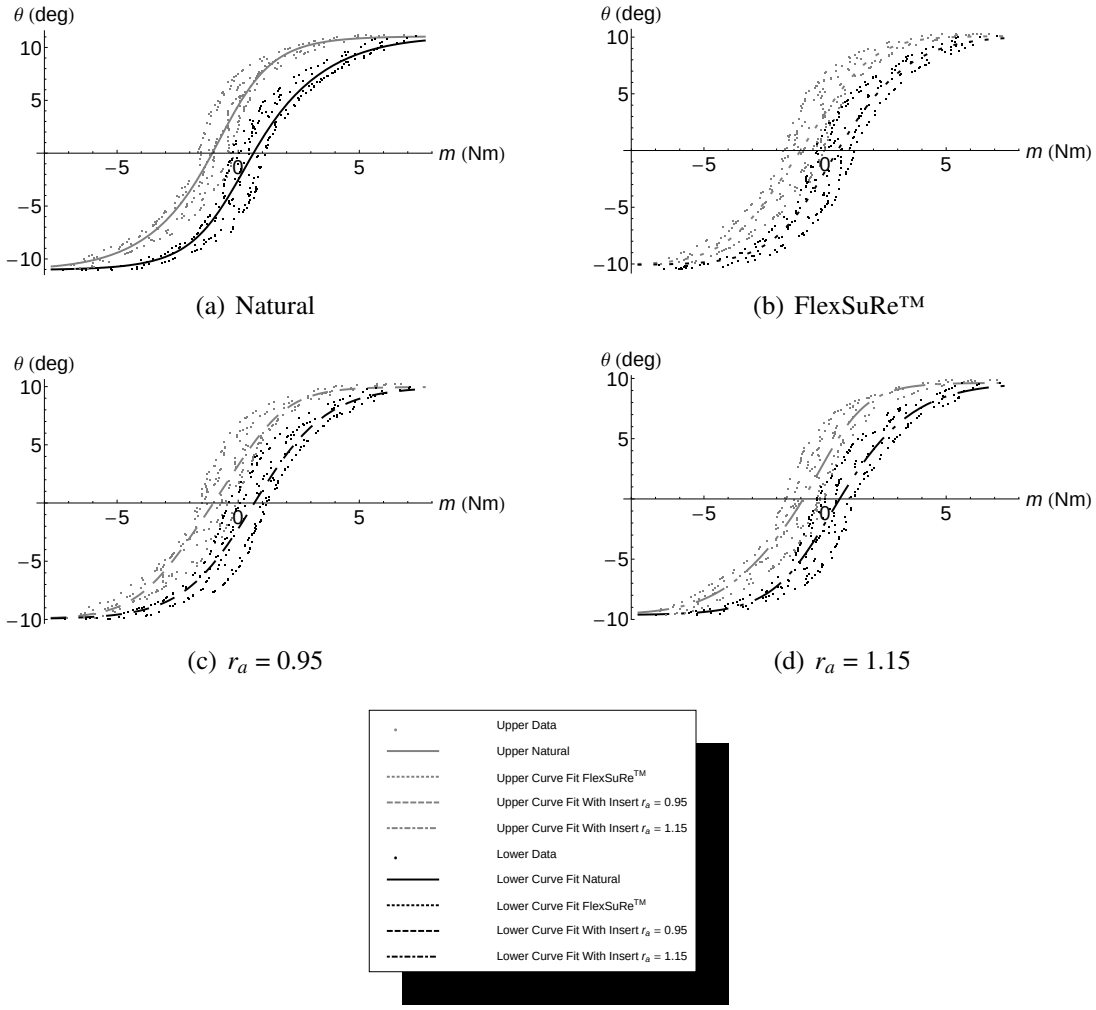

(a) Natural

(b) FlexSuRe™

(c) $r_a = 0.95$

(d) $r_a = 1.15$

(e) Legend

Figure 5.2: Lateral-bending data and curve fit

Table 5.3: Fit values for axial-rotation data

Test	Curve	A	B	$\alpha 1$	$m1$	$\alpha 2$	$m2$	R^2	Variance
AR Natural	Upper	-2.405	2.405	0.781053	-4.01619	0.665487	2.04392	0.99536	0.00746962
AR Natural	Lower	-2.405	2.405	0.409869	1.81168	0.411607	1.54803	0.984992	0.0297514
AR FlexSuRe	Upper	-2.420	2.420	0.687299	-3.96626	0.590865	1.65315	0.997482	0.00466871
AR FlexSuRe	Lower	-2.420	2.420	0.392379	1.40599	0.406635	0.7813	0.992966	0.0125815
AR $r_a = 0.95$	Upper	-2.325	2.325	0.406048	-0.745665	0.396588	-0.983392	0.993057	0.0110228
AR $r_a = 0.95$	Lower	-2.325	2.325	0.722445	4.1636	0.593628	-1.29209	0.998049	0.00357746
AR $r_a = 1.15$	Upper	-2.395	2.395	0.662986	-3.77051	0.56928	1.95513	0.998132	0.00296366
AR $r_a = 1.15$	Lower	-2.395	2.395	0.644653	-1.56381	0.661408	4.08738	0.997244	0.00486316

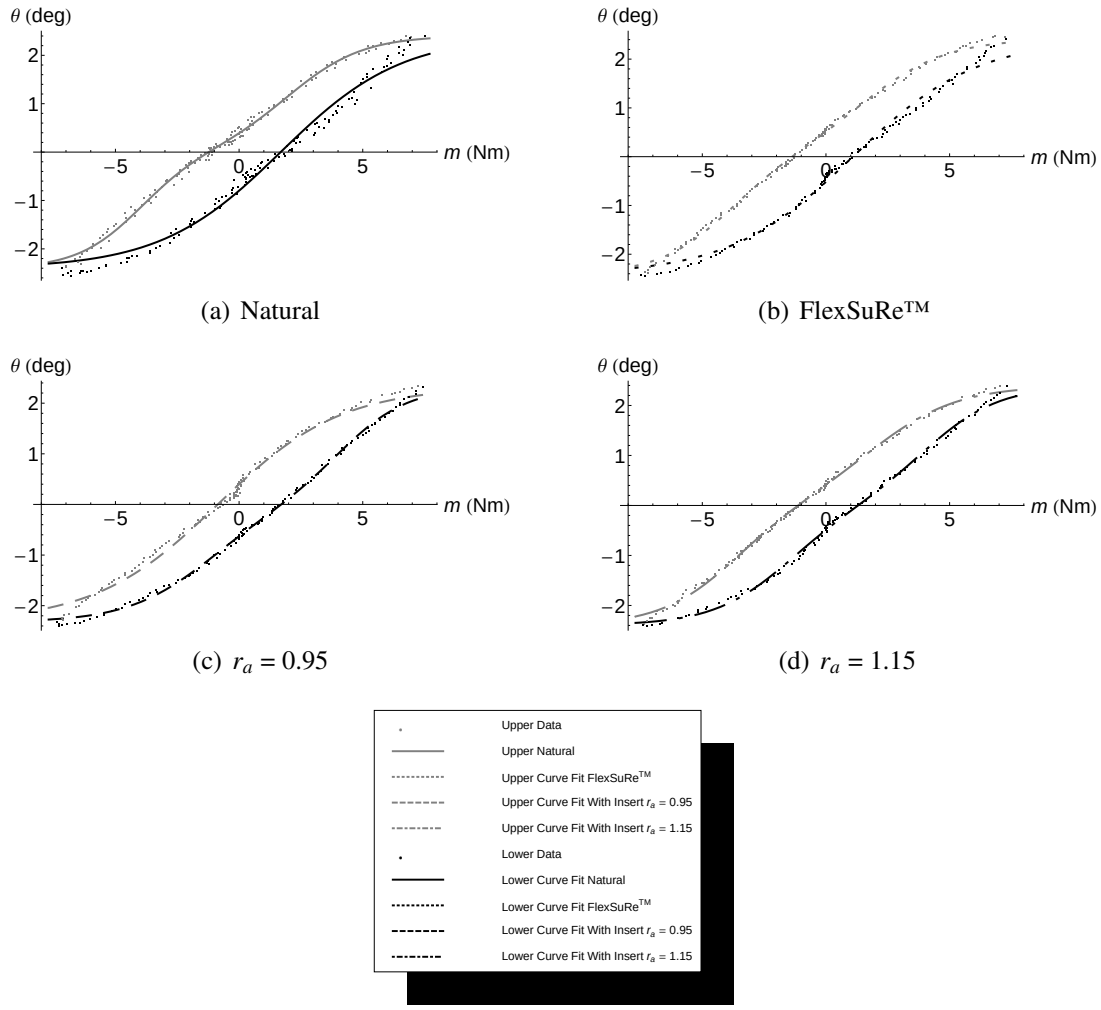

(a) Natural (b) FlexSuRe™

(c) $r_a = 0.95$ (d) $r_a = 1.15$

(e) Legend

Figure 5.3: Axial-rotation data and curve fit

for each fit and the *Knz*. Stiffness increases when the ROM decreases or the *Knz* increases. It was expected that the device would increase the stiffness of the FSU.

Flexion-extension shows increased stiffness as can be observed by the ROM decreasing from 14.6 deg to 8.6 deg, and the *Knz* increasing from 0.29 N-m/deg to 0.82 N-m/deg for the upper curve and from 0.34 N-m/deg to 0.71 N-m/deg for the lower curve. Lateral-bending increases in stiffness but is less significant with a ROM decrease from 22.1 deg to 19.3 deg and a *Knz* increase from 0.25 N-m/deg to 0.32 N-m/deg for the upper curve and from 0.27 N-m/deg to 0.32 N-m/deg for the lower curve. Axial-rotation was least effected with ROM remaining at 4.8 deg and the *Knz* changing from 2.59 N-m/deg to 2.54 N-m/deg for the upper curve and from 2.03 N-m/deg

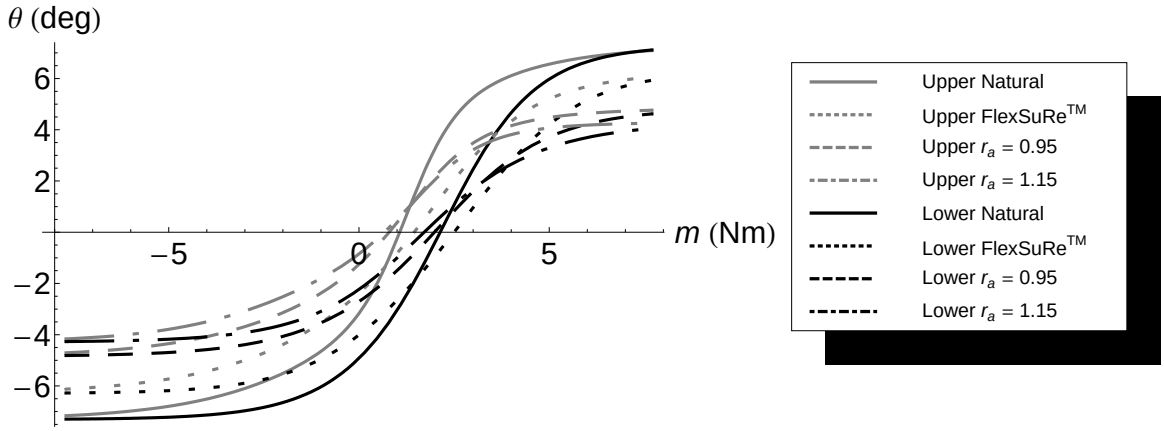

Figure 5.4: Flexion-extension curve fits compared

Table 5.4: Comparison of fit values for flexion-extension data with respect to natural disc

Test	Curve	ROM (deg)	*Knz* (N-m/deg)
FE Natural	Upper	14.6	0.29
FE FlexSuRe	Upper	12.6	0.57
FE r_a = 0.95	Upper	9.7	0.64
FE r_a = 1.15	Upper	8.6	0.83
FE Natural	Lower	14.6	0.34
FE FlexSuRe	Lower	12.6	0.54
FE r_a = 0.95	Lower	9.7	0.63
FE r_a = 1.15	Lower	8.6	0.71

to 2.48 N-m/deg for the lower curve. The change in axial-rotation may not be significant. It was also noted that the curve fit for the axial-rotation is not a tight fit, especially for the ends of the curve, notwithstanding its high R^2 term. The raw data was superimposed for each loading case for axial-rotation and there is little effect on the axial stiffness (see Figure 5.7).

Tables 5.4 and 5.5 show a steady increase of stiffness from natural, to FlexSuRe™ , to the first insert, to the second insert. These results show that as predicted, increasing the r_a value of the inserts increases stiffness of the FSU. The values listed in Table 5.6 show that unlike the other loading conditions there is no pattern to the change in stiffness for axial rotation, and the different values are most likely due to noise. This is a significant finding considering that during the literature review in chapter 2 it was sown that Axial rotation has the largest correlation of

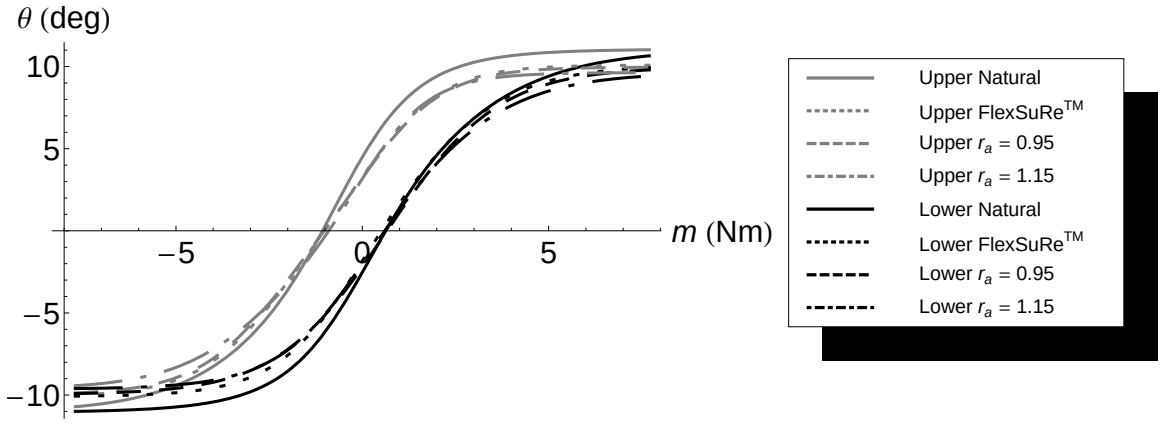

Figure 5.5: lateral-bending curve fits compared

Table 5.5: Comparison of fit values for Lateral-bending data with respect to natural disc

Test	Curve	ROM (deg)	*Knz* (N-m/deg)
LB Natural	Upper	22.1	0.25
LB FlexSuRe	Upper	20.2	0.32
LB r_a = 0.95	Upper	19.9	0.33
LB r_a = 1.15	Upper	19.3	0.32
LB Natural	Lower	22.1	0.27
LB FlexSuRe	Lower	20.2	0.30
LB r_a = 0.95	Lower	19.9	0.30
LB r_a = 1.15	Lower	19.3	0.32

decreased stiffness for degeneration. Figures 2.3 and 2.4 show that axial rotation has the strongest trend for increased joint laxity due to degeneration.

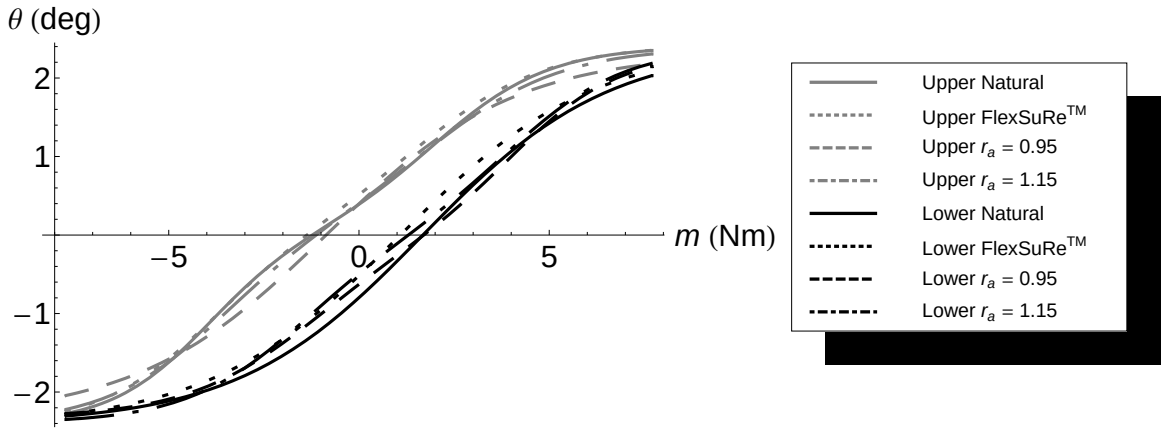

Figure 5.6: Axial-rotation curve fits compared

Table 5.6: Comparison of fit values for axial-rotation data with respect to natural disc

Test	Curve	ROM (deg)	*Knz* (N-m/deg)
AR Natural	Upper	4.8	2.59
AR FlexSuRe	Upper	4.8	2.46
AR $r_a = 0.95$	Upper	4.7	2.15
AR $r_a = 1.15$	Upper	4.8	2.54
AR Natural	Lower	4.8	2.03
AR FlexSuRe	Lower	4.8	2.08
AR $r_a = 0.95$	Lower	4.7	2.49
AR $r_a = 1.15$	Lower	4.8	2.48

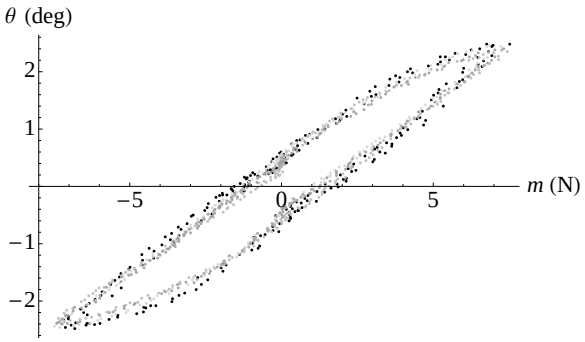

Figure 5.7: Axial-rotation raw data overlaid using gray scale differentiation.

CHAPTER 6. DEVELOPMENT OF THE SPAR BY REDUCING DEVICE SIZE THROUGH GEOMETRIC OPTIMIZATION

6.1 Introduction

The contact-aided FlexSuRe™ spinal implant provided nonlinear force-deflection characteristics that resembled the response of the spine while providing customizable stiffness. However, it is necessary to alter the design to reduce the size to facilitate its use in-vivo. It was proposed that if it could be miniaturized while maintaining a LET joint geometry, then the contact-aided device could be made smaller and provide the needed force-deflection response and alterability. Additionally, other limitations of the FlexSuRe™that were targeted for improvement were torque on the pedicle screws, and stiffness in axial-rotation loading conditions.

Concept generation and selection were performed using many ideas explained in Chapter 3. Most of the ideas for reducing the size involved transforming the member's geometry, orientation or position. After exploring the possibilities using selection criterion of feasibility, functionality, manufacturability, and strain energy capacity, the design that emerged victorious was that of a serpentine version of the LET joint. It incorporated multiple flexures and bases attached in series with one post on either end attached directly to the last flexure. The number of serpentine curves was varied and the best design for achieving the objectives was chosen for optimization. Figure 6.1 illustrates this design. After some design optimization it was determined that the stress in the bases were a limiting factor so they were changed to curved segments (Figure 6.1). The resulting device was called the Serpentine sPinal stAbility Restoration Device or the SPAR Device.

This chapter discusses the approach used to find feasible geometries that meet specific design criteria. Three unique geometries were developed which would fulfill three design objectives: i) a reaction force of 14 N at a displacement of 2 mm, ii) volume within 12x12x15 mm while providing a 100 N reaction force at a 2 mm deflection, and iii) geometry necessary to obtain 200 N of reaction force at 2 mm displacement with a preload providing a 100 N reaction force.

6.2 Set Up

Figure 6.1 shows the geometry of the device with the design variables defined (tl, $tl2$, $tl3$, bl, $bl2$, $bl3$, sh) Note that because of device symmetry the variables apply to both the top and bottom half. One additional dimension was $width$ of the beams, which is measured in the y direction. The device was displacement loaded for the analysis. The dimensions bl, $bl2$, $bl3$ could be any value so long as the initial position was not greater than a max height hm. Height above the max height hm was defined as del, this value was pre-deflected to create preload before the displacement load of $del2$ =2 mm was applied. The torsion lengths tl, $tl2$, $tl3$, and $width$ were constrained such that the x and y dimensions did not exceed bm. Constraints were added to ensure that the flexures and bases never touched. To do this, the base length constraints, bl, were conservatively defined such that

$$bl \geq (sh + 1/3 * (del2)) \tag{6.1}$$

or

$$(bl - sh) \leq 1/3 * (del2) \tag{6.2}$$

These equations were evaluated for each bl, $bl2$, $bl3$ creating three other terms: $blMsh$, $bl2Msh$, $bl3Msh$. Figure 6.1 illustrates how the constraint works. Note that the length bl runs along the centerline of the beam, leaving lengths of $sh/2$ above and below each end. These new terms were constrained as

$$del2 * 2/3 \leq blMsh \leq hm \tag{6.3}$$

The constraint that ensured del would eliminate any height that passed hm was the constraint *BaseSum* defined as

$$BaseSum = hm - 2 * (bl + bl2 + bl3) - del \tag{6.4}$$

and constrained such that,

$$0 \leq BaseSum \leq hm \tag{6.5}$$

The ends were fixed in all degrees of freedom, with one end being deflected in the z direction.

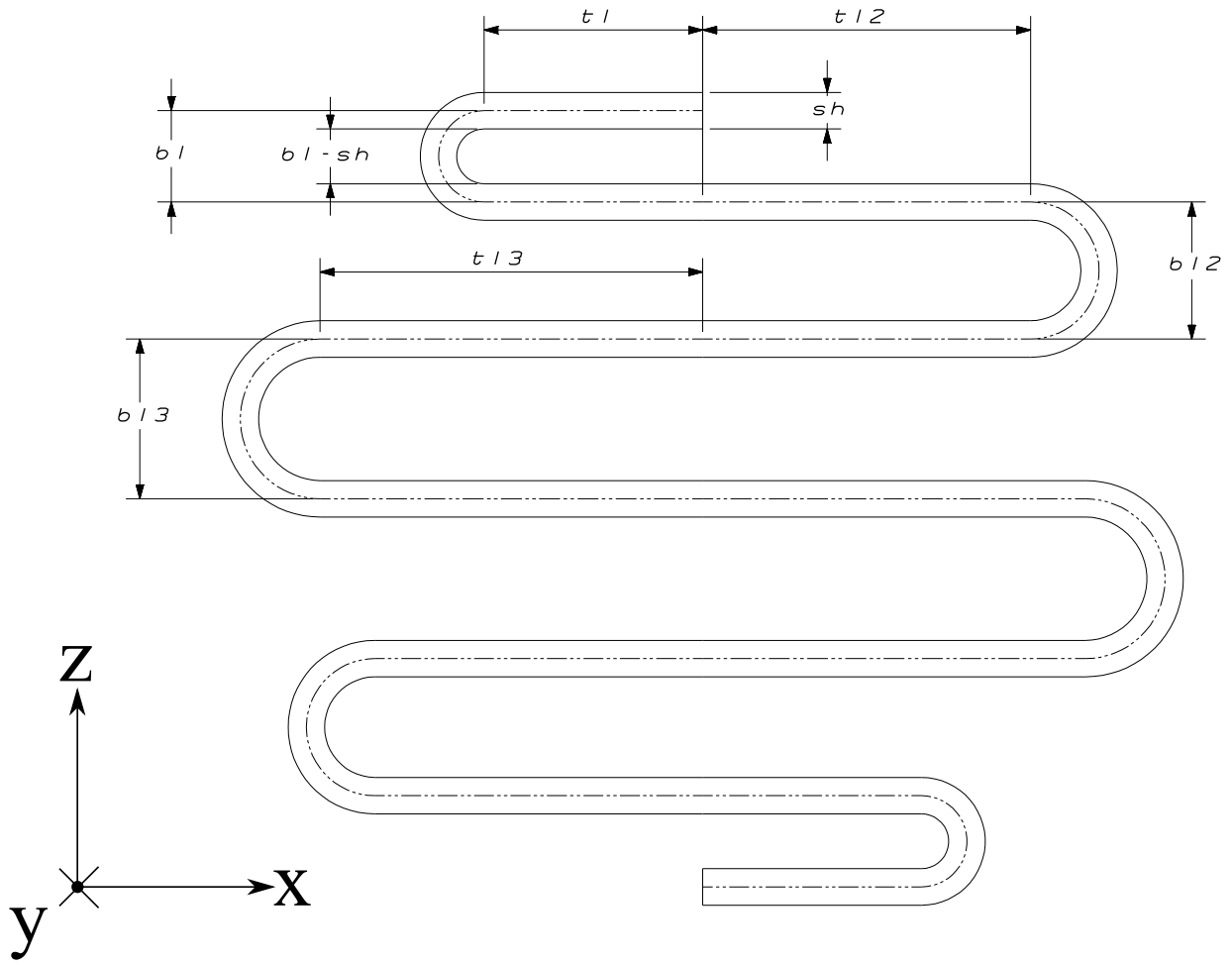

Figure 6.1: Serpentine geometry defined

An ANSYS batch file was created to model the device using finite element analysis. This file was referenced in Isight a commercial optimization program. The batch file defined the basic geometry, the displacement conditions and constraints and is included in Appendix C. The geometry was defined by the centerline geometry and beam3 elements were meshed onto the centerline. Titanium's material properties were used and can be seen in Table 6.1. The reaction force in the Z direction and the maximum stress were the output variables. Isight was used to change the design variables within the batch file, run the file within ANSYS in batch mode, acquire the resulting forces and stresses and then repeat. Analysis and design functions were defined in Isight with bounds set. Isight ran this loop while searching for an optimum using the Non-Linear Sequential Quadratic Programming (NLPQL) algorithm. The variables and functions for the optimization are

Table 6.1: Analysis and design variables, analysis and design functions.

Design Variables		Design Functions	
$width$	0.1 mm $\leq$ $width$ $\leq$ 12 mm	$stress$	$stress \leq 0.5 * Sy$
sh (Standard height)	0.1 mm $\leq$ sh $\leq$ 2 mm	$force1$	Target:(0 N, 100 N)
del (Initial deiplacement)	0.0 mm $\leq$ del $\leq$ 10 mm	$stress2$	$stress \leq 0.5 * Sy$
tl (Flexure top bottom)	2 mm $\leq$ tl $\leq$ 6 mm	$force2$	Target:(14 N, 200 N) or Maximize
$tl2$ (Flexure end middle)	2 mm $\leq$ $tl2$ $\leq$ 6 mm	Base sum	$0 \leq basesum \leq hm$
$tl3$(Flexure mid middle)	2 mm $\leq$ $tl3$ $\leq$ 6 mm	$blMsh$	$del2 * 2/3 \leq blMsh \leq hm$
bl(Base top bottom)	1 mm $\leq$ bl $\leq$ 6 mm	$bl2Msh$	$del2 * 2/3 \leq bl2Msh \leq hm$
$bl2$ (Base end middle)	1 mm $\leq$ $bl2$ $\leq$ 6 mm	$bl3Msh$	$del2 * 2/3 \leq bl3Msh \leq hm$
$bl3$(Base mid middle)	1 mm $\leq$ $bl3$ $\leq$ 6 mm		
Analysis Variables		**Analysis Functions**	
bm (Base max.)	$= 12$	a (Cross-sec. area)	$= width * sh$
hm (Height max.)	$= 15$	i (Moment of inertia)	$= width * sh^3/12$
e (Youngs modulus)	$= 113.8E6kPa$	$Basesum$	$= hm - 2 * (bl + bl2 + bl3) - del$
n (Poissons ratio)	$= 0.342$	$blMsh$	$= bl - sh$
$del2$ (Displacement)	$= -2mm$	$bl2Msh$	$= bl2 - sh$
Sy (Yield stress)	$= 8.8E5kPa$	$bl3Msh$	$= bl3 - sh$

listed in Table 6.1. Constraints were set such that the stress of the device could not exceed half the yield stress, and the output force was being optimized for objectives i, ii, and iii.

6.3 Procedure

The procedure for finding optimums for the three design objectives followed a pattern of determining a starting position, optimizing, verifying the result, and making observations about the design space at the optimum. A suitable starting point for the optimizer's algorithm was acquired using two methods. The first method entailed varying the geometry in trial and error within the ANSYS GUI. Once values close to the desired force was reached, the resulting dimensions became the starting point for the Isight optimization.

The second method was the use of discrete optimization through the Design of Experiments (DOE) workbench in Isight. This workbench evaluated the model at all combinations of user-entered values of each variable. This method was similar to an exhaustive search, however the entire design space was not explored. This workbench approximates the design space with a function, viewable on a contour plot (see Figure 6.2). It verified that $width$ and sh had the greatest effect on $force$ and $stress$, therefore these were the variables used in the contour plots. The software was not capable of providing boundaries on the contour plots; nevertheless, the designers

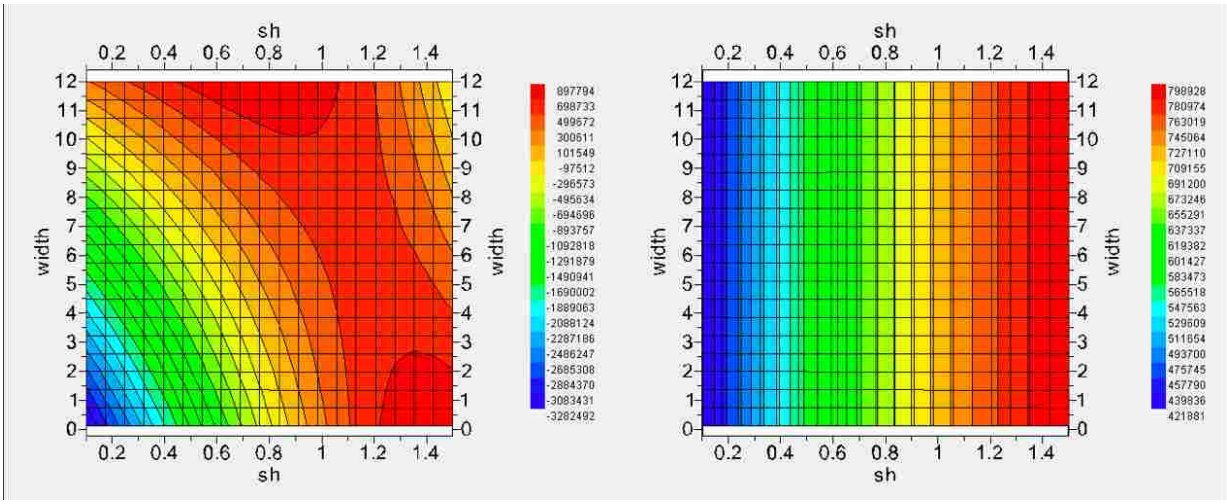

Figure 6.2: Design space plots with contours of force on the left plot and stress on the right.

used the plots to readjust the combinations of variables to better capture the feasible region. The adjustable variables were bl, $bl2$, $bl3$, tl, $tl2$ and $tl3$. The best values obtained within the most feasible region from this discrete analysis became the starting point for a continuous optimization. Figure 6.2 shows an example of two of the design space plots, evaluated at the best combination of variables from the DOE workbench. The plots have x and y values of sh vs. $width$, with contours of $force$ and $stress$. The function approximating the design space provided a useful overall picture of the relationship between variables, and a sufficiently good approximation for a starting point.

After a starting point was determined, the NLPQL algorithm was used for optimization. The starting values and final optimized values for the two methods are shown in Table 6.2. It was observed that both methods produced adequate starting positions. It was observed however that there were multiple local optimums with similar fitness.

For validation and visualization purposes, one of the designs was modeled in NX. The part was meshed using tetrahedral elements. A non-linear Nastran FEA simulation was run and the stress result obtained. This result is shown in Figure 6.3. The ANSYS model and the NX model predicted the same stress and force output for the given configuration.

It was observed that the optimums occurred at locations with very steep gradients implying that the optimum is a constrained optimum.

Table 6.2: Optimums found using two starting point acquisition methods.

Variable	Start 1	Optimum 1	Start 2	Optimum 2
width	12 mm	12 mm	12 mm	12 mm
sh	0.906 mm	0.792 mm	0.57 mm	0.788 mm
tl	5.95 mm	4.83 mm	3.5 mm	5.04 mm
tl2	6.37 mm	6.0 mm	6.0 mm	6.00 mm
tl3	7.03 mm	6.0 mm	6.0 mm	6.00 mm
bl	1.57 mm	1.46 mm	1.0 mm	1.45 mm
bl2	2.60 mm	4.58 mm	1.0 mm	4.20 mm
bl3	3.33 mm	1.46 mm	2.5 mm	1.84 mm
Force	-99,900 mN	-92,100 mN	-46,300 mN	-88,700 mN
Stress	441,000 kPa	440,000 kPa	428,000 kPa	440,000 kPa

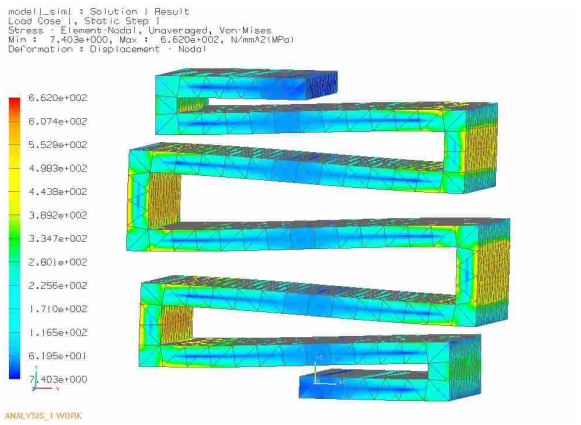

Figure 6.3: NX Nastran visualization verifying ANSYS results

6.4 Results of Three Optimization Scenarios

The optimization procedure was followed for three different scenarios. Objective i) had a target force ($force2$) of $14N$ with and minimized the geometric variables tl, $tl2$, $tl3$, bl, $bl2$, $bl3$, sh and $width$. Objective ii) maximized force for the previously mentioned geometric constraints. Objective iii) was split into two similar objectives. Objective iiia) had a target pre-load force ($force1$) of $100N$ and maximized force at the final deflection ($force2$), while maintaining the geometric constraints of 15 mm in x, 15 mm in y, and 15 mm in z. Objective iiib) used the same pre-load force objectives as iiia) and maximized the final deflection force ($force2$) while

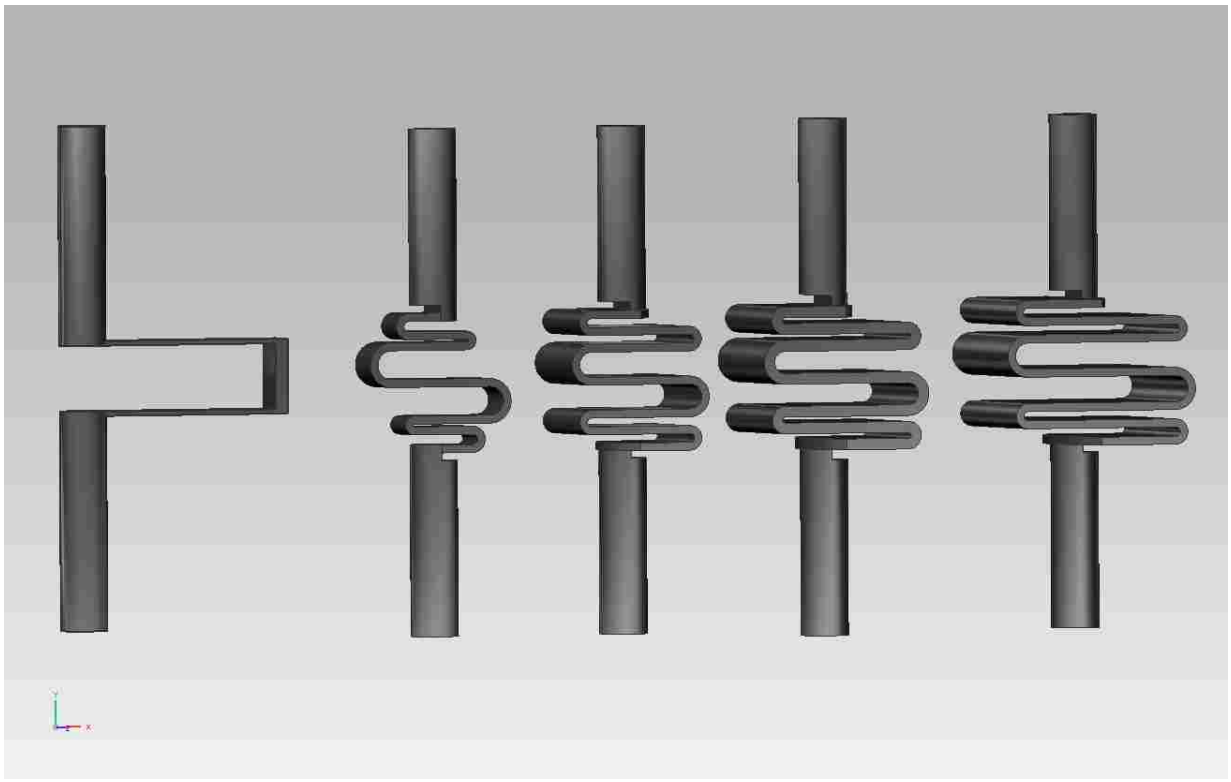

Figure 6.4: Optimized designs compared geometrically to original design. Design: original ,1, 2, 3a, 3b

maintaining the geometric constraints of 18 mm in x, 18 mm in y, and 15 mm in z. The values for the geometric dimensions for each optimized configuration are shown in Table 6.3 and the different configurations are compared geometrically to the original design of the FlexSuRe™ in Figure 6.4. The geometry can be much smaller using the serpentine configuration, while still providing the same axial force-deflection profile (compare original to design 1 in Figure 6.4). It was also shown that the serpentine design can attain very stiff force-deflection characteristics, while fitting in the design restraints of 12 mm in x and y and being able to deflect the necessary 2 mm (compare original to design 2 in Figure 6.4). If the geometric constraints are relaxed by 3 mm and 6 mm in the x and y direction while maintaining the geometric constraint in the z direction, a much stiffer device is possible attaining up to 191.5 N at final deflection or 38.6 N of force at preload and 246.2 N of force at final deflection (compare original to design 3a and 3b respectively in figure 6.4).

The design of the SPAR targeted eliminating multiple limitations to the FlexSuRe™'s baseline configuration. Size was the largest consideration and this design target was able to be met

Table 6.3: Optimized designs from differing objectives.

	Scenario			
Objective	1	2	3a	3b
width	4.88 mm	12 mm	15 mm	18 m
sh	0.55 mm	0.91 mm	1.29 mm	1.45 mm
tl	3.87 mm	6.00 mm	7.5 mm	9.0 mm
tl2	3.24 mm	6.00 mm	7.5 mm	9.0 mm
tl3	6.00 mm	6.00 mm	7.5 mm	9.0 mm
bl	2.09 mm	1.58 mm	1.95 mm	2.12 mm
bl2	1.22 mm	1.58 mm	1.95 mm	2.12 mm
bl3	4.19 mm	4.40 mm	3.59 mm	3.46 mm
del	0 mm	-0.1 mm	0.0 mm	-0.37 mm
Force	0 N	4.45 N	4.35 N	38.6 N
Stress	0 Pa	21.0 MPa	10.0 MPa	68.8 MPa
Force2	13.96 N	93.4 N	191.5 N	246.2 N
Stress2	422 MPa	440 MPa	440 MPa	440 MPa

satisfactorily. Torque on the pedicle screws was effectively eliminated by incorporating symmetry into the design. Lastly, it is predicted that axial rotation of the spine will be positively affected by this device due to its ability to rotate about the post's axis. If the flexures are positioned perpendicular to the direction of the FlexSuRe™'s flexures it will significantly increase stiffness in this mode of loading. Moreover, the device can be rotated at any angle between 0° and 90° to achieve a tailorable stiffness in axial rotation. Additional exploration of this characteristic is recommended.

CHAPTER 7. CONCLUSION AND RECOMMENDATIONS

The product development process for incorporating adjustability and non linearity to the FlexSuRe™ has been presented. Research of current technologies, the background of the FlexSuRe™, and current literature on degeneration of the spinal disc was used in the establishment of design requirements. The literature review concluded that there has been no study which has tested for and quantified individual torque-rotation curves based on levels of degeneration for the spine. This type of test would aid in understanding how the torque-rotation curve changes for different levels of degeneration for each section of the spine. Testing must be performed in which the torque-rotation curves for each spinal segment are considered with respect to their individual levels of degeneration. Due to the nature of the data being collected and because the testing is performed in-vitro, a follower load should be applied to simulate in-vivo conditions. [31] This testing was performed by others in parallel with the work in this thesis.

The implant requirements included adjustability and nonlinear stiffness that resembles spinal force-deflection. These requirements were successfully integrated into the FlexSuRe™ through the use of inserts for the original device. The inserts were modeled and the results demonstrated how different inserts could be used to created different behaviors, which could lead to customization for individual patient needs. The analytical model has been verified by FEA and physical tests and is available for the design of future implants.

Testing on a in-house spine tester showed that the FlexSuRe™ spinal implant and the inserts increase the stiffness of the FSU for flexion-extension and lateral-bending. It was observed that the stiffness in axial rotation was not measurably different from the natural condition. It was observed that the inserts added additional stiffness in flexion-extension. In lateral-bending the added stiffness was also observed; however, it was less pronounced. A negligible difference was observed in axial rotation, which was contributed to the loading direction of the implant during this motion. Evaluation of the device based on the functional requirements are shown in Table 7.1.

Table 7.1: Evaluation of FlexuRe™ According to Functional Requirements

Design Requirement	Results
Biocompatibility	The FlexSuRe™and SPAR have been designed for Ti-6AL-4V, which is a common spinal arthroplasty device material. The contact-aided inserts can be made using a Titanium alloy or a polymer such as PEEK which are common spinal arthroplasty device materials.
Minimal wear	The baseline device produces no wear due to being a fully compliant mechanisms. The inserts are intended to have constant contact which also includes no slip, thus wear will be negligible.
Infinite fatigue life	The fatigue strength for Ti-6Al-4V is $S = 510$ MPa at $10E6$ cycles. This device is predicted to deflect 2 mm and will reach a stress of 388 MPa at that deflection. It will reach a stress of 441 MPa at that deflection with a contact insert of $r_a = 1.00$. The SPAR is designed to undergo 440 MPa at the same deflection.
Share compressive loads with the spinal segment	At the predicted 2 mm deflection, the baseline FlexSuRe™ will have a reaction load of 24 N and a reaction load of 30.4 N with the insert of $r_a = 1.00$. The SPAR will have a reaction load of 93.4 N for scenario 2. Both device's geometry can be altered to increase or decrease this value.
Surgical placement	The FlexSuRe™ fits between pedicle screws and is of comparable size to StabiliMax™. The baseline device has sharp edges and a possible pinch site between posts. However, the attachments cover the flexures such that there are no sharp edges exposed and greatly reduces the possibility for pinching to occur. The SPAR is smaller and fits into the surgeon-advisory-board-prescribed window of 12 x12 x 15 mm.
Restore healthy spinal kinematics	The FlexSuRe™ was shown capable of restoring ROM and preserving the natural helical axis of rotation by maintaining interpedicular travel. Physical testing of the SPAR will be required for this evaluation.
Duplicate healthy spinal kinetics	The FlexSuRe™ with inserts is capable of producing a sigmoidal response similar to the healthy spine. Moreover, this device has been shown to restore stiffness and can be designed for the needs of the individual. However, the FlexSuRe™ did not show the ability to restore stiffness to the axial rotation direction of loading. The SPAR is based of the same models and should produce the same results, however, due to its size it has the ability to be oriented such that axial stiffness would be increased. Additionally, the contact-aided inserts can be designed to be used in conjunction with the SPAR for nonlinear results.
No pedicle screw loosening	FlexSuRe™ induces a moment load on the pedicle screw of 0.065 Nm at 2 mm of deflection. With inserts r_a= 1.00 it induces a moment load of 0.074 Nm. The SPAR is symmetric about the axis connecting the two pedicle screws and thus should induce no moment load for lateral bending and flexion-extension, axial rotation may induce a moment load and the magnitude should be experimentally determined.
Tailorable	Multiple baseline devices can be made with different stiffnesses and the inserts can provide the range between baseline models. Alterations after implantation would not require the entire device to be removed, and changes could be achieved leaving the pedicle assembly intact and changing out the contact-aided attachment.
Manufacturability	Both devices were manufactured using Wire Electrical-Discharge-Machining (EDM) and the SPAR would require milling and turning operations as well. The contact-aided inserts can be manufactured using wire EDM or injection molding, depending on material selection.

The need to reduce the device size was realized during the development of the implant . Abstraction of the device concept was used during further concept development of the device and a new concept of LET joints in series with a serpentine-like profile was selected. This new geometry was optimized to find specific force-deflection characteristics and reduce the size. The results of the optimization showed that the serpentine geometry can attain the same force-deflection capabilities in compression as the original design while reducing the size of the device to be less than 12 x 12 x 15 mm. Additionally, it was demonstrated that the serpentine device can provide stiffer conditions and still achieve the necessary deflection. It is proposed that the new geometry would positively affect the stiffness of the spinal segment in axial rotation due to its geometry and size, allowing it to be rotated about its post and positioned in any direction. It is recommended that further exploration be accomplished by using a genetic algorithm with three objectives: maximizing reaction forces at 2 mm deflection, setting a target reaction force during preload, and minimizing geometry. From these three objectives a pareto front could be defined which would better explore the possibilities of the design. Evaluation of this version of the device is also listed in Table 7.1.

Future work can use the demonstrated contact-aided design as well as the serpentine geometry to further develop the device so that it corrects the degenerated condition, provides an environment in which degeneration can be slowed or stopped, and possibly provide an environment which facilitates regeneration. Additionally, studies should be performed which establish the change in kinetics and kinematics due to conventional spinal surgeries. This study would provide information that would aid in developing the devices so that they could help during the healing process after such surgeries. Additional testing could be done which gradually dissects a cadaveric spine to assess the contributions of ligaments and facets in the motion pattern, thus defining a target for the design of the devices for each condition.

Future development of the device should included non-invasive alterability of either the contact-aided inserts or the baseline devices. Remote actuation to change the r_a value of the inserts would increase or decrease stiffness. More testing of the device could include placing the spinal devices into the spine tester without a spine (perhaps using sawbones with no facets) to find the reactions in all modes of loading. This testing would give further insight into modes of parasitic motion that the device may be experiencing while in vivo.

REFERENCES

[1] Ong, K., Lau, E., Ianuzzi, A., Villaraga, M., and Kurtz, S., 2008. "Future demand in spinal fsions: US projections to 2030." In *Scientific Exhibit 75th Annual Meeting of the American Associations of Orthopaedic Surgeons* San Francisco, CA.

[2] Ullrich, P. F. Lumbar degenerative disc disease: Causes, symptoms, diagnosis and treatment http://www.spine-health.com/conditions/degenerative-disc-disease/lumbar-degenerative-disc-disease.

[3] Schizas, C., Duff, J. M., Tessitore, E., and Faundez, A., 2009. "Non fusion techniques in spinal surgery." *Revue Médicale Suisse,* **5**(230), Dec., pp. 2574–2577 PMID: 20085207.

[4] Selard, E., Shirazi-Adl, A., and Urban, J. P. G., 2003. "Finite element study of nutrient diffusion in the human intervertebral disc." *Spine,* **28**(17), Sept., pp. 1945–1953; discussion 1953 PMID: 12973139.

[5] Urban, J. P. G., Smith, S., and Fairbank, J. C. T., 2004. "Nutrition of the intervertebral disc." *Spine,* **29**(23), Dec., pp. 2700–2709 PMID: 15564919.

[6] Stratton, E., Howell, L. L., and Bowden, A. "Force-displacement model of the flexsure™ spinal implant." *Proceedings of the ASME International Design Engineering Technical Conferences*, Aug. 15-18, 2010, DETC2010- 28476.

[7] Panjabi, M. M., Oxland, T. R., Yamamoto, I., and Crisco, J. J., 1994. "Mechanical behavior of the human lumbar and lumbosacral spine as shown by three-dimensional load-displacement curves." *The Journal of Bone and Joint Surgery. American Volume,* **76**(3), Mar., pp. 413–424 PMID: 8126047.

[8] Panjabi, M. M., Goel, V., Oxland, T., Takata, K., Duranceau, J., Krag, M., and Price, M., 1992. "Human lumbar vertebrae quantitative three-dimensional anatomy." *SPINE,* **17**(3), pp. 299–306.

[9] Natarajan, R. N., and Andersson, G. B. J., 1999. "The influence of lumbar disc height and cross- sectional area on the mechanical response of the disc to physiologic loading." *SPINE,* **24**(18), pp. 1873–1881.

[10] Mimura, M., 1994. "Disc degeneration affects the multidirectional flexibility of the lumbar spine." *Spine,* **19**(12), pp. 1371–1380.

[11] Stokes, I. A. F., and Iatridis, J. C., 2004. "Mechanical conditions that accelerate intervertebral disc degeneration: overload versus immobilization." *Spine,* **29**(23), Dec., pp. 2724–2732 PMID: 15564921.

[12] Oskouian, R. J., Whitehill, R., Samii, A., Shaffrey, M. E., Johnson, J. P., and Shaffrey, C. I., 2004. "The future of spinal arthroplasty: a biomaterial perspective." *Neurosurgical Focus,* **17**(3), Sept., p. E2 PMID: 15636558.

[13] Hellier, W. G., Hedman, T. P., and Kostuik, J. P., 1992. "Wear studies for development of an intervertebral disc prosthesis." *Spine,* **17**(6).

[14] Kurtz, S. M., van Ooij, A., Ross, R., de Waal Malefijt, J., Peloza, J., Ciccarelli, L., and Villarraga, M. L. "Polyethylene wear and rim fracture in total disc arthroplasty." *The Spine Journal,* **7**(1), Jan., pp. 12–21.

[15] van Ooij, A., Kurtz, S. M., Stessels, F., Noten, H., and van Rhijn, L., 2007. "Polyethylene wear debris and long-term clinical failure of the charité disc prosthesis: A study of 4 patients." *Spine,* **32**(2).

[16] Hirakawa, K., Bauer, T. W., Stulberg, B. N., and Wilde, A. H., 1996. "Comparison and quantitation of wear debris of failed total hip and total knee arthroplasty." *Journal of Biomedical Materials Research,* **31**(2), June, pp. 257–263.

[17] Wasielewski, R. C., Galante, J. O., Leighty, R. M., Natarajan, R. N., and Rosenberg, A. G., 1994. "Wear patterns on retrieved polyethylene tibial inserts and their relationship to technical considerations during total knee arthroplasty." *Clinical Orthopaedics and Related Research,* **299**.

[18] Dumbleton, J. H., Manley, M. T., and Edidin, A. A., 2002. "A literature review of the association between wear rate and osteolysis in total hip arthroplasty." *The Journal of Arthroplasty,* **17**(5), Aug., pp. 649–661.

[19] Ambati, D. V., 2010. "Effect of design variables on biomechanics of lumbar spine implanted with single, multilevel and hybrid posterior dynamic stabilization systems." thesis.

[20] Ahn, Y., Chen, W., Lee, K., Park, K., and Lee, S., 2008. "Comparison of the load-sharing characteristics between pedicle-based dynamic and rigid rod devices." *Biomedical Materials,* **3**(4), Dec., p. 044101.

[21] Hilibrand, A. S., and Robbins, M., 2004. "Adjacent segment degeneration and adjacent segment disease: the consequences of spinal fusion?." *The Spine Journal: Official Journal of the North American Spine Society,* **4**(6 Suppl), Dec., pp. 190S–194S PMID: 15541666.

[22] Park, P., Garton, H. J., Gala, V. C., Hoff, J. T., and McGillicuddy, J. E., 2004. "Adjacent segment disease after lumbar or lumbosacral fusion: Review of the literature." *Spine,* **29**(17).

[23] Gertzbein, S. D., Seligman, J., Holtby, R., Chan, K. H., Kapasouri, A., Tile, M., and Cruickshank, B., 1985. "Centrode patterns and segmental instability in degenerative disc disease." *Spine,* **10**(3), Apr., pp. 257–261 PMID: 3992346.

[24] Miyazaki, M., Hong, S. W., Yoon, S. H., Zou, J., Tow, B., Alanay, A., Abitbol, J., and Wang, J. C., 2008. "Kinematic analysis of the relationship between the grade of disc degeneration and motion unit of the cervical spine." *Spine,* **33**(2), pp. 187–193 PMID: 18197105.

[25] Hudson, W. R., Gee, J. E., Billys, J. B., and Castellvi, A. E., 2011. "Hybrid dynamic stabilization with posterior spinal fusion in the lumbar spine." *SAS Journal,* **5**(2), June, pp. 36–43.

[26] Castellvi, A. E., Huang, H., Vestgaarden, T., Saigal, S., Clabeaux, D. H., and Pienkowski, D., 2007. "Stress reduction in adjacent level discs via dynamic instrumentation: A finite element analysis." *SAS Journal,* **1**(2), June, pp. 74–81.

[27] Yue, J. J., Timm, J. P., Panjabi, M. M., and La Torre, J. J., 2007. "Clinical application of the panjabi neutral zone hypothesis: the stabilimax NZ posterior lumbar dynamic stabilization system." *Neurosurgical FOCUS,* **22**(1), Jan., pp. 1–3.

[28] BENDER, T J, J., 1955. "Mechanical basis of low back pain." *Journal of the Medical Association of the State of Alabama,* **24**(9), Mar., pp. 217–218 PMID: 14354414.

[29] Goel, P. Measuring bending moment induced in lumbar pedicle screws.

[30] Okuyama, K., Abe, E., Suzuki, T., Tamura, Y., Chiba, M., and Sato, K., 2000. "Can insertional torque predict screw loosening and related failures?: An in vivo study of pedicle screw fixation augmenting posterior lumbar interbody fusion." *Spine,* **25**(7).

[31] Patwardhan, A. G., Havey, R. M., Carandang, G., Simonds, J., Voronov, L. I., Ghanayem, A. J., Meade, K. P., Gavin, T. M., and Paxinos, O., 2003. "Effect of compressive follower preload on the flexion-extension response of the human lumbar spine." *Journal of Orthopaedic Research: Official Publication of the Orthopaedic Research Society,* **21**(3), May, pp. 540–546 PMID: 12706029.

[32] Krismer, M., Haid, C., Behensky, H., Kapfinger, P., Landauer, F., and Rachbauer, F., 2000. "Motion in lumbar functional spine units during side bending and axial rotation moments depending on the degree of degeneration." *Spine,* **25**(16), Aug., pp. 2020–2027 PMID: 10954631.

[33] Tanaka, N., An, H. S., Lim, T. H., Fujiwara, A., Jeon, C. H., and Haughton, V. M., 2001. "The relationship between disc degeneration and flexibility of the lumbar spine." *The Spine Journal: Official Journal of the North American Spine Society,* **1**(1), Feb., pp. 47–56 PMID: 14588368.

[34] Fujiwara, A., Lim, T. H., An, H. S., Tanaka, N., Jeon, C. H., Andersson, G. B., and Haughton, V. M., 2000. "The effect of disc degeneration and facet joint osteoarthritis on the segmental flexibility of the lumbar spine." *Spine,* **25**(23), Dec., pp. 3036–3044 PMID: 11145815.

[35] Grogan, J., 1997. "Lumbar facet joint tropism does not accelerate degeneration of the facet joints." *American Journal of Neuroradiology,* **18**, August, pp. 1325–1329.

[36] Soini, J., Antti-Poika, I., Tallroth, K., Konttinen, Y. T., Honkanen, V., and Santavirta, S., 1991. "Disc degeneration and angular movement of the lumbar spine: Comparative study using plain and Flexion-Extension radiography and discography." *Journal of Spinal Disorders June 1991,* **4**(2), pp. 183–187.

[37] Kurowski, P., and Kubo, A., 1986. "The relationship of degeneration of the intervertebral disc to mechanical loading conditions on lumbar vertebrae." *Spine,* **11**(7), Sept., pp. 726–731 PMID: 3787344.

[38] Niosi, C. A., and Oxland, T. R., 2004. "Degenerative mechanics of the lumbar spine." *The Spine Journal,* **4**(6, Supplement 1), Nov., pp. S202–S208.

[39] An, H. S., 1996. "The relationsip between disc degeneration and kinematic characteristics of lumbar motion segment." In *11th Annual Meeting of North American Spine Society*.

[40] Umehara, S., Tadano, S., Abumi, K., Katagiri, K., Kaneda, K., and Ukai, T., 1996. "Effects of degeneration on the elastic modulus distribution in the lumbar intervertebral disc." *Spine,* **21**(7), Apr., pp. 811–819; discussion 820 PMID: 8779011.

[41] Seligman, J. V., Gertzbein, S. D., Tile, M., and Kapasouri, A., 1984. "Computer analysis of spinal segment motion in degenerative disc disease with and without axial loading." *Spine,* **9**(6), Sept., pp. 566–573 PMID: 6495026.

[42] Campana, S., de Guise, J., Rillardon, L., Mitton, D., and Skalli, W., 2007. "Lumbar intervertebral disc mobility: effect of disc degradation and of geometry." *European Journal of Orthopaedic Surgery & Traumatology,* **17**(6), Nov., pp. 533–541.

[43] Bible, J. E., Simpson, A. K., Emerson, J. W., Biswas, D., and Grauer, J. N., 2008. "Quantifying the effects of degeneration and other patient factors on lumbar segmental range of motion using multivariate analysis." *Spine,* **33**(16).

[44] Friberg, S., and Hirsch, C., 1992. "Anatomical and clinical studies on lumbar disc degeneration. 1950." *Clinical Orthopaedics and Related Research*(279), June, pp. 3–7 PMID: 1600669.

[45] Paajanen, H., Erkintalo, M., Dahlstrm, S., Kuusela, T., Svedstrm, E., and Kormano, M., 1989. "Disc degeneration and lumbar instability. magnetic resonance examination of 16 patients." *Acta Orthopaedica Scandinavica,* **60**(4), Aug., pp. 375–378 PMID: 2816310.

[46] Farfan, H. F., Huberdeau, R. M., and Dubow, H. I., 1972. "Lumbar intervertebral disc degeneration: the ingluence of geometrical geatures on the pattern of disc degeneration–a post mortem study." *J Bone Joint Surg Am,* **54**(3), Apr., pp. 492–510.

[47] Schnake, K. J., Putzier, M., Haas, N. P., and Kandziora, F., 2006. "Mechanical concepts for disc regeneration." *European Spine Journal,* **15**(Suppl 3), Aug., pp. 354–360 PMID: 16835733 PMCID: 2335380.

[48] Penning, L., Wilmink, J. T., and van Woerden, H. H., 1984. "Inability to prove instability. a critical appraisal of clinical-radiological flexion-extension studies in lumbar disc degeneration." *Diagnostic Imaging in Clinical Medicine,* **53**(4), pp. 186–192 PMID: 6236010.

[49] Panjabi, M. M., Krag, M. H., and Chung, T. Q., 1984. "Effects of disc injury on mechanical behavior of the human spine." *Spine,* **9**(7), Oct., pp. 707–713 PMID: 6505841.

[50] Kirkaldy-Willis, W. H., and Farfan, H. F., 1982. "Instability of the lumbar spine." *Clinical Orthopaedics and Related Research,* **165**.

[51] Stokes, I. A. F., and Frymoyer, J. W., 1987. "Segmental motion and instability." *Spine,* **12**(7).

[52] Haughton, V. M., Schmidt, T. A., Keele, K., An, H. S., and Lim, T. H., 2000. "Flexibility of lumbar spinal motion segments correlated to type of tears in the annulus fibrosus." *Journal of Neurosurgery,* **92**(1 Suppl), pp. 81–86 PMID: 10616062.

[53] Guan, Y., Yoganandan, N., Moore, J., Pintar, F. A., Zhang, J., Maiman, D. J., and Laud, P., 2007. "Moment-rotation responses of the human lumbosacral spinal column." *Journal of Biomechanics,* **40**(9), pp. 1975–1980 PMID: 17101141.

[54] Pennal, G. F., Conn, G. S., McDonald, G., Dale, G., and Garside, H., 1972. "Motion studies of the lumbar spine: a preliminary report." *The Journal of Bone and Joint Surgery. British Volume,* **54**(3), Aug., pp. 442–452 PMID: 5053887.

[55] Yamamoto, I., Panjabi, M. M., Crisco, T., and Oxland, T., 1989. "Three-dimensional movements of the whole lumbar spine and lumbosacral joint." *Spine,* **14**(11), Nov., pp. 1256–1260 PMID: 2603060.

[56] Schultz, A., Warwick, D., Berkson, M., and Nachemson, A., 1979. "Mechanical properties of human lumbar spine motion segments- responses in flexion, extension, lateral bending, and torsion." *Journal of Biomechanical Engineering,* **101**(1), pp. 46–52 Compendex.

[57] Quack, C., Schenk, P., Laeubli, T., Spillmann, S., Hodler, J., Michel, B. A., and Klipstein, A., 2007. "Do MRI findings correlate with mobility tests? an explorative analysis of the test validity with regard to structure." *European Spine Journal: Official Publication of the European Spine Society, the European Spinal Deformity Society, and the European Section of the Cervical Spine Research Society,* **16**(6), June, pp. 803–812 PMID: 17143634.

[58] Howell, L. L., 2001. *Compliant Mechanisms*. John Wiley & Sons, New York, NY.

[59] Jacobsen, J. O., Howell, L. L., and Magleby, S. P., 2010. "Lamina emergent mechanisms and their basic elements." *Journal of Mechanisms and Robotics,* **2**(1), pp. 011003–1 to 011003–9.

[60] Mankame, N. D., and Ananthasuresh, G. K., 2001. "Synthesis of contact-aided compliant mechanisms for non-smooth path generation." *International Journal for Numerical Methods in Engineering,* **69**(12), March 19, pp. 2564–2605.

[61] Mankame, N. D., and Ananthasuresh, G. K., 2004. "Topology optimization for synthesis of contact-aided compliant mechanisms using regularized contact modeling." *Computers and Structures,* **82**(15-16), June, pp. 1267–1290.

[62] Cannon, J. R., and Howell, L. L., 2005. "A compliant contact-aided revolute joint." *Mechanism and Machine Theory,* **40**(11), pp. 1273–1293.

[63] Halverson, P. A., Howell, L. L., and Magleby, S. P., 2010. "Tension-based multi-stable compliant rolling-contact elements." *Mechanism & Machine Theory,* **45**(2), pp. 147–156.

[64] Mehta, V., Frecker, M., and Lesieutre, G. A., 2009. "Stress relief in Contact-Aided compliant cellular mechanisms." *Journal of Mechanical Design,* **131**(9), pp. 091009–11.

[65] Moon, Y.-M., 2007. "Bio-mimetic design of finger mechanism with contact aided compliant mechanism." *Mechanism and Machine Theory,* **42**(5), May, pp. 600–611.

[66] Mankame, N. D., and Ananthasuresh, G. K., 2007. "A compliant transmission mechanism with intermittent contacts for cycle-doubling." *Journal of Mechanical Design,* **129**(1), January, pp. 114–121.

[67] Halverson, P. A., Howell, L. L., and Bowden, A. E. "A flexure-based bi-axial contact-aided compliant mechanism for spinal arthroplasty." *Proceedings of the 32nd Annual Mechanisms & Robotics Conference at the 2008 ASME International Design Engineering Technical Conferences,* Aug. 3-6, 2008, DETC2008-50121.

[68] Shoup, T. E., and McLarnan, C. W., 1971. "On the use of the undulating elastica for the analysis of flexible link mechanisms." *J. Engineering for Industry,* **93**, Feb., pp. 263–267.

[69] Zirbel, S. A., Stolworthy, D. K., Howell, L. L., and Bowden, A. E., (In Review). "Standardized characterization of lumbar segmental response using a dual inflection point boltzmann sigmoid." *International Journal for Numerical Methods in Biomedical Engineering*.

APPENDIX A. ANSYS BATCH FILE FOR CONTACT-AIDED MODEL

```
FINISH
/CLEAR,START
/COM,ANSYS RELEASE 11.0    UP20070125       13:45:05    03/25/2010

!Entering the Preperation mode
/PREP7


! Define constants
! Ultimate Yield Stress is 880e6 Pa

! Constants
nelem=500
b=.004
h=.0005
a=b*h
i=b*h*h*h/12
e=113.8e9
n=.342
l=.020
PI=ACOS(-1)
rad = 2*l

! displacements
del=-1.8896141E-3
steps=25

! Creating Keypoints
K,1,0,l/8,0,
K,2,l,l/8,0,

! Creating a Line between Keypoints
L,1,2

! Defining the local element type as a 3D beam
ET,1,BEAM3
R,1,a,i,h

! Defining material properties
MP,EX,1,e
MP,prxy,1,n

! Meshing the line
LESIZE,All, , ,nelem/2, ,1, , ,1,
LMESH,All

! define the contact surface
!!!Elllipse
LOCAL,11,1,,,,,,,0.15625  ! PAR1 argument is key for creating elliptical
CSYSCSYS,11       !go the the local coordinant system 11
K,3:8,L/1.25,0:90:18     !Create the keypoints 3-8 with a radius of L/8,
              using degrees 0-90 in incraments of 18 deg.
bspline,3,4,5,6,7,8   ! Create a line using 6 keypoints to curve fit the line

!!!Circle
!k,4,0,l/8,0,
```

```
!k,5,0,l/8-rad,0
!k,6,rad,l/8-rad,0

!larc,4,6,5,rad


!!!!! Contact creation


/COM, CONTACT PAIR CREATION - START
CM,_NODECM,NODE
CM,_ELEMCM,ELEM
CM,_KPCM,KP
CM,_LINECM,LINE
CM,_AREACM,AREA
CM,_VOLUCM,VOLU
/GSAV,cwz,gsav,,temp
MP,MU,1,.1
MAT,1
MP,EMIS,1,7.88860905221e-031
R,3
REAL,3
ET,2,169
ET,3,172
R,3,,,10.0,0.001,0,
RMORE,,,1.0E20,0.0,1.0,
RMORE,0.0,0,1.0,,1.0,0.5
RMORE,0,1.0,1.0,0.0,,1.0
KEYOPT,3,3,0
KEYOPT,3,4,0
KEYOPT,3,5,0
KEYOPT,3,7,0
KEYOPT,3,8,0
KEYOPT,3,9,0
KEYOPT,3,10,2
KEYOPT,3,11,0
KEYOPT,3,12,0
KEYOPT,3,2,0
KEYOPT,2,2,0
KEYOPT,2,3,0
! Generate the target surface
LSEL,S,,,2
CM,_TARGET,LINE
TYPE,2
LATT,-1,3,2,-1
TYPE,2
LMESH,ALL
! Generate the contact surface
LSEL,S,,,1
CM,_CONTACT,LINE
TYPE,3
NSLL,S,1
ESLN,S,0
ESURF
*SET,_REALID,3
ALLSEL
ESEL,ALL
ESEL,S,TYPE,,2
ESEL,A,TYPE,,3
ESEL,R,REAL,,3
LSEL,S,REAL,,3
/PSYMB,ESYS,1
/PNUM,TYPE,1
/NUM,1
EPLOT
! Reverse target normals
!CM,_Y,LINE
!LSEL, , , ,       2
```

```
!CM,_YEL,ELEM
!CM,_YND,NODE
!NSLL,S,1
!ESLN,S,1
!ESEL,R,REAL,,_REALID
!ESURF,,REVERSE
!CMSEL,S,_Y
!CMSEL,S,_YEL
!CMSEL,S,_YND
!CMDELE,_Y
!CMDELE,_YEL
!CMDELE,_YND
!/REPLOT
!*
ESEL,ALL
ESEL,S,TYPE,,2
ESEL,A,TYPE,,3
ESEL,R,REAL,,3
LSEL,S,REAL,,3
/PSYMB,ESYS,1
/PNUM,TYPE,1
/NUM,1
EPLOT
! Reverse contact normals
ESEL,NONE
ESEL,A,TYPE,,3
ESEL,R,REAL,,3
ESURF,,REVERSE
ESEL,ALL
ESEL,S,TYPE,,2
ESEL,A,TYPE,,3
ESEL,R,REAL,,3
LSEL,S,REAL,,3
/PSYMB,ESYS,1
/PNUM,TYPE,1
/NUM,1
EPLOT
!
ESEL,ALL
ESEL,S,TYPE,,2
ESEL,A,TYPE,,3
ESEL,R,REAL,,3
LSEL,S,REAL,,3
CMSEL,A,_NODECM
CMDEL,_NODECM
CMSEL,A,_ELEMCM
CMDEL,_ELEMCM
CMSEL,S,_KPCM
CMDEL,_KPCM
CMSEL,S,_LINECM
CMDEL,_LINECM
CMSEL,S,_AREACM
CMDEL,_AREACM
CMSEL,S,_VOLUCM
CMDEL,_VOLUCM
/GRES,cwz,gsav
CMDEL,_TARGET
CMDEL,_CONTACT
/COM, CONTACT PAIR CREATION - END

!!!!! End contact creation
finish


/solu

! input the boundary conditions and loads
```

```
! fix the left side (key piont 1)

ksel,s,kp,,1
nslk,s
d,all,all

! Displace the right side, no rotation, (keypiont 2)
ksel,s,kp,,2
nslk,s
d,all,rotz,0
d,all,uy,del

allsel,all

! set the solution options
ANTYPE,0 ! static analysis
NLGEOM,1 ! non-linear analysis
NSUBST,10,20,10 ! set the number of substeps, max, min
OUTRES,ALL,1 ! output the results at each substep
TIME,1  ! time at the end of the first loadstep

solve ! sovle the model

finish

/post1   ! entering post processing

set,last,last
PLDISP,1

!writing tables

ESEL,S,ENAME,,beam3
ETABLE,si,NMISC, 1
ETABLE,sj,NMISC, 3
ETABLE,Uj,

allsel,all

ESEL,S,ENAME,,conta172

ETABLE,sli,NMISC, 9
ETABLE,slj,NMISC, 10
ETABLE,gpi,NMISC, 5
ETABLE,gpj,NMISC, 6

presol,cont


!*********************************************

! deffineing tables to be filed
*get,sub_st,active,0,solu,ncmss

*dim,xdis,table,sub_st
*dim,ydis,table,sub_st
*dim,yforce,table,sub_st
!allsel,all

! GET THE FORCE SUM AT THE displaced node

*Do,dd,1,sub_st,1
set,1,dd
*get,disx,node,2,U,x
*get,disy,node,2,U,y
*GET,forceY,node,2,rf,fy
*SET,xdis(DD),disx
```

```
*SET,ydis(DD),disY
*SET,Yforce(DD),forceY
*Enddo
ALLSEL,ALL

!*****************************************

! writing the output file

/output,dispVforce.txt
*Do,dd,1,sub_st,1
*VWRITE,xdis(dd,1),ydis(dd,1),yforce(dd,1)
%16.8G %16.8G %16.8G
*ENDDO
/output

FINISH

ESEL,S,ENAME,,beam3
```

APPENDIX B. MATHEMATICA CODE FOR CONTACT-AIDED MODEL

B.1 Ellipse Defined

```
Ellipse2[l_, h_, k_, a_, b_, di_, \[CapitalEpsilon]_, w_, t_] :=
 Module[{output, po, x1, x, h1, k1, r1, a1, b1, y1, f, f\[Theta], s,
   M, n, i, j, L, \[CapitalIota], c, \[Sigma]},
  If[l < a, L = l, L = a - di];
  \[CapitalIota] = (w t^3)/12;
  c = t/2;
  f[x1_, h1_, k1_, a1_, b1_] =
   y1 /. Solve[(x1 - h1)^2/a1^2 + (y1 - k1)^2/b1^2 == 1, y1][[2]];

  f\[Theta][x1_, h1_, k1_, a1_, b1_] =
   ArcTan[D[f[x1, h1, k1, a1, b1], x1]];

  po = Transpose[{Range[0, L, di],
     Table[f[x, h, k, a, b], {x, 0, L, di}]}];
  n = Length[po];
  s[x1_, a1_, b1_] = (
   a1 Sqrt[1 - x1^2/a1^2] Sqrt[(a1^4 - a1^2 x1^2 + b1^2 x1^2)/(
    a1^4 - a1^2 x1^2)] EllipticE[ArcSin[x1/a1], 1 - b1^2/a1^2])/Sqrt[
   1 - x1^2/a1^2 + (b1^2 x1^2)/a1^4];
  M[x1_, h1_, k1_, a1_,
    b1_] = (\[CapitalEpsilon] \[CapitalIota] D[
     f\[Theta][x1, h1, k1, a1, b1], x1])/D[s[x1, a1, b1], x1];
  output =
   Transpose[{Range[0, L, di], Table[f[x, h, k, a, b], {x, 0, L, di}],
      Table[s[x, a, b], {x, 0, L, di}],
     Table[f\[Theta][x, h, k, a, b], {x, 0, L, di}],
     Table[M[x, h, k, a, b], {x, 0, L, di}],
     Table[(M[x, h, k, a, b] c)/\[CapitalIota], {x, 0, L, di}]}]
  (*Output is in the form {x,y,s,f\[Theta],M,\[Sigma]}*)
  ]
```

B.2 Contact-Aided Cantilevered Beam

```
CA::usage =
  "CA[[lt,x,ra,rb,\[CapitalEpsilon],w,t]={FP,Q,\[Delta],\[Sigma]} \
returns a list of four elements, a plot of the beam in its current \
deflection FP, the force required to deflect to that position Q, the \
amount of deflection \[Delta], and the max stres in the beam \
\[Sigma].  The input required is, length of overall beam lt, x \
position of the lift off location, ellipse width as a percent of \
total length ra, ellipse height as a percent of total length rb, \
Youngs modulus E, width of beam w and thickness of beam t. ";

CA[lt_, x_, ra_, rb_, \[CapitalEpsilon]_, w_, t_] :=
 Module[{a, b, Cs, n, L, \[Alpha]1, \[Alpha]2, P, M2, LP1, Cs2,
   ContFunc, s1, s2, sQ, s4, W, H, M1, sk, \[Phi]1, \[Phi]2, Q, n2,
   tt, p1, Tx, Ty, Txy, LP2, LP3, FP, frn, \[CapitalIota],
```

```
   c, \[Sigma], k, Ry, p, kt},

  (*Initial set up*)
  \[CapitalIota] = (w t^3)/12;
  c = t/2;
  (*frn=.76;*)
  a = ra;(*ellipse width*)
  b = rb;(*ellipse height*)

    Cs = Ellipse2[x, 0, 0, a, b, .0001, \[CapitalEpsilon], w,
    t];(*Running Ellipse1 program*)

  n = Length[
    Cs];(*Length of matrix containing values from Ellipse program*)

  L = lt - Cs[[n, 3]];(*Length of free part of beam*)
  \[Alpha]1 =
   0;(*Angle at guided end of beam*)
  \[Alpha]2 = -Cs[[n,
     4]];(*Angle at contact end of beam*)
  P = 0;(*Horizontal force*)

    M2 = Cs[[n, 5]];(*Moment at contact end of beam*)

  LP1 = ListLinePlot[Transpose[{Cs[[All, 1]], Cs[[All, 2]]}],
    PlotRange -> {{0, a}, {0, b}},
    PlotStyle -> { Thick, Gray, Dotted}, Filling -> Axis];

  (*Plot of contact surface*)

  Cs2 = Ellipse2[a - .0001, 0, 0, a, b, .0001, \[CapitalEpsilon], w,
    t];
  (*ContFunc=Interpolation[Transpose[{Cs[[All,1]],Cs[[All,
  2]]}]];*)
  (*Print[a,b,n,L,\[Alpha]1,\[Alpha]2,P,M2,LP1,
  ContFunc]*)

  (*Defining Functions*)

  s1 = \[Phi]1a -> ArcSin[1/(Sqrt[2] k)];(*Lower limit of integration*)

    s2 = \[Phi]2a -> \[Pi] -
     ArcSin[Sqrt[1 + Sin[\[Alpha]2]]/(
      Sqrt[2] k)];(*Upper limit of integration*)

  sQ = Qa -> M2^2/(
     4 k^2 \[CapitalEpsilon] \[CapitalIota] Cos[\[Phi]2a]^2) /. \
{s2};(*Vertical Force*)

  (*Print[s1,s2,sQ]*)

  s4[k_] = (-L (Qa^2)^(1/4)/
        Sqrt[\[CapitalEpsilon] \[CapitalIota]]) + (EllipticF[\[Phi]2a,
         k^2] - EllipticF[\[Phi]1a, k^2]) /. {s1, s2,
     sQ};(*Function defining k*)
  (*Print[s4[k]]*)

  (*Elliptic Integrals*)


  W[\[Phi]2a_] =
   W1 /. Solve[
      0 == (-W1 (P^2 + Q^2)^(3/4)/
           Sqrt[\[CapitalEpsilon] \[CapitalIota]]) +
```

```
      P (2 EllipticE[\[Phi]2a, k^2] - 2 EllipticE[\[Phi]1a, k^2] -
         EllipticF[\[Phi]2a, k^2] + EllipticF[\[Phi]1a, k^2]) +
      2 k Q (Cos[\[Phi]2a] - Cos[\[Phi]1a]), W1][[1]];

H[\[Phi]2a_] =
 H1 /. Solve[
    0 == (-H1 (P^2 + Q^2)^(3/4)/
         Sqrt[\[CapitalEpsilon] \[CapitalIota]]) +
      Q (2 EllipticE[\[Phi]2a, k^2] - 2 EllipticE[\[Phi]1a, k^2] -
         EllipticF[\[Phi]2a, k^2] + EllipticF[\[Phi]1a, k^2]) +
      2 k P (Cos[\[Phi]2a] - Cos[\[Phi]1a]), H1][[1]];


(*Secondary Definitions*)

M1 = 2 k Sqrt[\[CapitalEpsilon] \[CapitalIota] Q] Cos[\[Phi]1a];

(*Print[s4[
k]];*)
(*This is a plot of k values to get a better guess.*)
\
(*p1=Plot[s4[k],{k,-1,1},PlotRange->All(*{{-1,1},{-5,5}}*),
ImageSize-> 500];*)

kt = Table[{k, s4[k]}, {k, 0.0001, .9999, .0001}];
p = Position[kt[[All, 2]],
   Select[kt[[All, 2]], Im[#] == 0 &, 1][[1]]][[1, 1]];
frn = kt[[p, 1]];

sk = FindRoot[s4[k], {k, frn}][[1]];


If[Abs[Im[k /. sk]] > 0,
 While[Abs[Im[k /. sk]] > 0 && frn < 1,
   frn = frn + .01;
   sk = FindRoot[s4[k], {k, frn}][[1]];
   Print[{sk, frn}];
          ]
  If[frn == 1,
   frn = .76;
   While[Abs[Im[k /. sk]] > 0 && frn > 0,
    frn = frn - .01;
    sk = FindRoot[s4[k], {k, frn}][[1]];
    Print[{sk, frn}]
             ]
     ]

  ];

\[Phi]1 = \[Phi]1a //. {s1, sk};
\[Phi]2 = \[Phi]2a //. {s2, sk};
Q = Qa //. {sQ, sk};
(*Print[W[\[Phi]]/.s1/.sk,H[\[Phi]]/.s1/.sk,
sk]*)
(*Stress*)
\[Sigma] = (M1 c)/\[CapitalIota] //. {s1, sk};

(*Plotting*)

n2 = Length[Cs2];
tt = Transpose[{Cs2[[n ;; n2, 1]], Cs2[[n ;; n2, 2]]}];
Tx = Table[
  W[\[Phi]2a] + Cs[[n, 1]] - W[\[Phi]2] /. s1 /.
   sk, {\[Phi]2a, \[Phi]1, \[Phi]2, .01}];
Ty = Table[-H[\[Phi]2a] + Cs[[n, 2]] + H[\[Phi]2] /. s1 /.
   sk, {\[Phi]2a, \[Phi]1, \[Phi]2, .01}];
```

```
Txy = Sort[Transpose[{Tx, Ty}]];
LP2 = ListLinePlot[Txy, PlotStyle -> {Thick, Gray}];
LP3 = ListLinePlot[tt, PlotRange -> {{0, a*1.25}, {0, b}},
  PlotStyle -> {LightGray}, Filling -> Axis];
Ry = If[Ty[[1]] < 0, Ty[[1]]*1.05, 0];
FP = Show[LP1, LP2, LP3, AspectRatio -> Automatic,
  PlotRange -> {{0, lt*1.25}, {Ry, Cs[[1, 2]]}},
  Ticks -> {{.005, .01, .015, .02, .025}, {0, .0005, .0015, .0025}},
   AxesLabel -> {"X (m)", "Y (m)"}, ImageSize -> 500];

(*{Q,b-Ty//First,\[Sigma]}*)
(*This is to be evaluated for the force and stress graphs*)
{FP, b - Ty[[1]], Q}
(*THis is to be evaluated for the position graphs*)
]
```

B.3 No Contact Cantilevered Beam

```
NoCA[Q_, P_, b_, lt_, \[CapitalEpsilon]_, w_, t_] :=

Module[{L, \[Alpha]1, \[Alpha]2, M1, s1, s2, M2, s4, W, H,
  sk, \[Phi]1, \[Phi]2, sT, n2, tt, p1, p2, Tx, Ty, Txy, LP5, FP,
  frn, \[CapitalIota], c, \[Sigma]},
(*Initial set up*)
\[CapitalIota] = (w t^3)/12;
c = t/2;
frn = .76;
L = lt;(*Length of free part of beam*)
\[Alpha]1 =
 0;(*angle at guided end*)
\[Alpha]2 =
 0;(*angle at fixed end*)

(*Defining Functions*)

M1 = 2 k Sqrt[\[CapitalEpsilon] \[CapitalIota] Qa]
   Cos[\[Phi]1a];(*Moment at guided end*)

s1 = \[Phi]1a ->
  ArcSin[ Cos[(\[Pi]/2 - \[Alpha]1)/2]/k];(*Lower integration limit*)

  s2 = \[Phi]2a -> \[Pi] -
   ArcSin[(1 + Sin[\[Alpha]2])^(
    1/2)/((2^(1/2)) k )];(*Upper integration limit*)

M2 = Solve[
   Mb == 2 k Sqrt[\[CapitalEpsilon] \[CapitalIota]] Qa^(1/2)
       Cos[\[Phi]2a] /. {s2}, Mb][[1,
  1]];(*Moment at fixed side*)
(*Print[s1,s2,M1,M2]*)

(*Elliptic Integral*)

s4[k_] = (-L (Qa^2)^(1/4)/
      Sqrt[\[CapitalEpsilon] \[CapitalIota]]) + (EllipticF[\[Phi]2a,
       k^2] - EllipticF[\[Phi]1a, k^2]) /. {s1, s2, M2, Qa -> Q};

(*Elliptic Integral*)

W[\[Phi]2a_] =
 W1 /. Solve[
```

```
    0 == (-W1 (Pa^2 + Qa^2)^(3/4)/
         Sqrt[\[CapitalEpsilon] \[CapitalIota]]) +
      Pa (2 EllipticE[\[Phi]2a, k^2] - 2 EllipticE[\[Phi]1a, k^2] -
         EllipticF[\[Phi]2a, k^2] + EllipticF[\[Phi]1a, k^2]) +
      2 k Qa (Cos[\[Phi]2a] - Cos[\[Phi]1]), W1][[1]];

H[\[Phi]2a_] =
 H1 /. Solve[
    0 == (-H1 (Pa^2 + Qa^2)^(3/4)/
         Sqrt[\[CapitalEpsilon] \[CapitalIota]]) +
      Qa (2 EllipticE[\[Phi]2a, k^2] - 2 EllipticE[\[Phi]1a, k^2] -
         EllipticF[\[Phi]2a, k^2] + EllipticF[\[Phi]1a, k^2]) +
      2 k Pa (Cos[\[Phi]2a] - Cos[\[Phi]1]), H1][[1]];
(*Print[H[\[Phi]]/.s1/.s2/.M2]*)

(*Secondary conditions*)

sk = FindRoot[s4[k], {k, frn}][[1]];

If[Abs[Im[k /. sk]] > 0,
 While[Abs[Im[k /. sk]] > 0 && frn < 1,
   frn = frn + .01;
   sk = FindRoot[s4[k], {k, frn}][[1]];
          ]
  If[frn == 1,
   frn = .76;
   While[Abs[Im[k /. sk]] > 0 && frn > 0,
    frn = frn - .01;
    sk = FindRoot[s4[k], {k, frn}][[1]];
             ]
     ]
 (*p1=Plot[s4[k],{k,0,1},PlotRange->{{0,1},{-5,5}},ImageSize->
 500];
 Print["Try new frn close to zero on plot.",
 p1]*)(*This is a plot of k values to get a better guess.*)
  ];

\[Phi]1 = \[Phi]1a //. {s1, sk};
\[Phi]2 = \[Phi]2a //. {s2, sk};
sT = { Qa -> Q, Pa -> P};
(*n2=Length[Cs2];*)
(*tt=Transpose[{Cs2[[n;;n2,1]],Cs2[[n;;n2,
2]]}];*)
(*ContTotalFunc=Interpolation[tt];*)
(*Print[
W[\[Phi]]/.sT/.s1/.sk,H[\[Phi]]/.s1/.sk,sk]*)

(*Stress*)
\[Sigma] = (M1 c)/\[CapitalIota] //. {s1, sk} //. sT;
(*Plots*)


p1 = Plot[s4[k], {k, 0, 1}, PlotRange -> {{0, 1}, {-5, 5}}];
p2 = ParametricPlot[{W[\[Phi]2a], H[\[Phi]2a]} /. sT /. s1 /.
   sk, {\[Phi]2a, \[Phi]1, \[Phi]2},
  PlotRange -> Automatic  (*{{-.03,.03},{-.01,.01}}*)];
Tx = Table[
  W[\[Phi]2a] - W[\[Phi]2] /. sT /. s1 /.
   sk, {\[Phi]2a, \[Phi]1, \[Phi]2, .01}];
Ty = Table[-H[\[Phi]2a] + b + H[\[Phi]2] /. sT /. s1 /.
   sk, {\[Phi]2a, \[Phi]1, \[Phi]2, .01}];
Txy = Sort[Transpose[{Tx, Ty}]];
LP5 = ListPlot[Txy, PlotStyle -> {Black, PointSize[.01]}];
FP = Show[LP5, AspectRatio -> Automatic,
```

```
  PlotRange -> Automatic(*{{0,lt+2 b},{0,a}}*)];
{FP, b - Ty // First, Q}(*{Q,b-Ty//First,\[Sigma]}*)

]
```

APPENDIX C. ANSYS BATCH FILE FOR OPTIMIZATION

```
!Entering the Preperation mode
/PREP7

! Define constants
! Ultimate Yield Stress is 880e6 Pa

! Constants
!Width is constant
width=12

!maximums (base and height)
bm=12
hm=15

!(standard height)
sh=4
!Beam props
a=width*sh
i=width*sh*sh*sh/12

! torsion width length, area, moment of inertia

!Flexure top bottom
tl=6
!Flexure end middle
tl2=6
!Flexure middle middle
tl3=6
!base top bottom
bl=1.5769
!base two end middle
bl2=1.5769
!base two middle middle
bl3=4.3962
!elastic modulus, and poissons ratio.
e=113.8e6
n=.342

!random constants
nelem=30
PI=ACOS(-1)

! displacements
del=hm-2*(bl+bl2+bl3)
del2=del-2

! Creating Keypoints
! one half let
K,1,0,0,0,
K,2,tl,0,0,
K,3,tl,bl,0,
K,4,0,bl,0,

!add another
K,5,-tl2,bl,0,
K,6,-tl2,bl+bl2,0,
```

```
K,7,0,bl+bl2,0,

!add a third
K,8,tl3,bl+bl2,0,
K,9,tl3,bl+bl2+bl3,0,
K,10,0,bl+bl2+bl3,0,

!add a fourth
K,11,-tl3,bl+bl2+bl3,0,
K,12,-tl3,bl+bl2+2*bl3,0,
K,13,0,bl+bl2+2*bl3,0,

!add a fifth
K,14,tl2,bl+bl2+2*bl3,0,
K,15,tl2,bl+2*bl2+2*bl3,0,
K,16,0,bl+2*bl2+2*bl3,0,

!add a sixth
K,17,-tl,bl+2*bl2+2*bl3,0,
K,18,-tl,2*bl+2*bl2+2*bl3,0,
K,19,0,2*bl+2*bl2+2*bl3,0,


!Arc Keypoints
k,20,tl+bl/2,bl/2,0
K,21,-tl2-bl2/2,bl+bl2/2,0,
K,22,tl3+bl3/2,bl+bl2+bl3/2,0,
K,23,-tl3-bl3/2,bl+bl2+bl3*3/2,0,
K,24,tl2+bl2/2,bl+bl2*3/2+2*bl3,0,
K,25,-tl-bl/2,bl*3/2+2*bl2+2*bl3,0,

k,26,tl,bl/2,0
K,27,-tl2,bl+bl2/2,0,
K,28,tl3,bl+bl2+bl3/2,0,
K,29,-tl3,bl+bl2+bl3*3/2,0,
K,30,tl2,bl+bl2*3/2+2*bl3,0,
K,31,-tl,bl*3/2+2*bl2+2*bl3,0,


! Creating a Line between Keypoints
!First let
L,1,2  !L1 torsion
!L,2,3  !L2 base
LARC,2,20,26,bl/2
LARC,20,3,26,bl/2
L,3,4  !L3 torsion

!second
L,4,5  !L4 torsion
!L,5,6  !L5 base2
LARC,5,21,27,bl2/2
LARC,21,6,27,bl2/2
L,6,7  !L6 torsion

!third
L,7,8  !L7 torsion
!L,8,9  !L8 base
LARC,8,22,28,bl3/2
LARC,22,9,28,bl3/2
L,9,10  !L9 torsion

!fourth
L,10,11  !L10 torsion
!L,11,12  !L11 base
LARC,11,23,29,bl3/2
LARC,23,12,29,bl3/2
L,12,13  !L12 torsion
```

```
!fifth
L,13,14  !L13 torsion
!L,14,15  !L14 base
LARC,14,24,30,bl2/2
LARC,24,15,30,bl2/2
L,15,16  !L15 torsion

!sixth
L,16,17  !L16 torsion
!L,17,18  !L17 base
LARC,17,25,31,bl/2
LARC,25,18,31,bl/2
L,18,19  !L18 torsion



! Defining the local element type as a 3D beam
! Defining material properties
MP,EX,1,e
MP,prxy,1,n
MP,dens,1,rho

! Defining the local element type as a 3D beam
ET,1,BEAM3
R,1,a,i,sh

!!!! Meshing base
!!!!Meshing  bases top bottom


Real,1

LESIZE,1, , ,nelem/2, ,1, , ,1,
LESIZE,2, , ,nelem/2, ,1, , ,1,
LESIZE,3, , ,nelem/2, ,1, , ,1,
LESIZE,4, , ,nelem/2, ,1, , ,1,
LESIZE,5, , ,nelem/2, ,1, , ,1,
LESIZE,6, , ,nelem/2, ,1, , ,1,
LESIZE,7, , ,nelem/2, ,1, , ,1,
LESIZE,8, , ,nelem/2, ,1, , ,1,
LESIZE,9, , ,nelem/2, ,1, , ,1,
LESIZE,10, , ,nelem/2, ,1, , ,1,
LESIZE,11, , ,nelem/2, ,1, , ,1,
LESIZE,12, , ,nelem/2, ,1, , ,1,
LESIZE,13, , ,nelem/2, ,1, , ,1,
LESIZE,14, , ,nelem/2, ,1, , ,1,
LESIZE,15, , ,nelem/2, ,1, , ,1,
LESIZE,16, , ,nelem/2, ,1, , ,1,
LESIZE,17, , ,nelem/2, ,1, , ,1,
LESIZE,18, , ,nelem/2, ,1, , ,1,
LESIZE,19, , ,nelem/2, ,1, , ,1,
LESIZE,20, , ,nelem/2, ,1, , ,1,
LESIZE,21, , ,nelem/2, ,1, , ,1,
LESIZE,22, , ,nelem/2, ,1, , ,1,
LESIZE,23, , ,nelem/2, ,1, , ,1,
LESIZE,24, , ,nelem/2, ,1, , ,1,

LMESH,1
LMESH,2
LMESH,3
LMESH,4
LMESH,5
LMESH,6
LMESH,7
LMESH,8
LMESH,9
```

```
LMESH,10
LMESH,11
LMESH,12
LMESH,13
LMESH,14
LMESH,15
LMESH,16
LMESH,17
LMESH,18
LMESH,19
LMESH,20
LMESH,21
LMESH,22
LMESH,23
LMESH,24


!*****************************************
!Solution!
/solu
!Specifying the analysis type
ANTYPE,0 ! static analysis

! input the boundary conditions and loads
NLGEOM,1 ! non-linear analysis

! fix keypoint 1
ksel,s,kp,,1
nslk,s
d,all,all,0



! Displace the top, no rotation, (keypoint 19)
ksel,s,kp,,19
nslk,s
d,all,rotz,0
d,all,ux,0
d,all,uy,del

!write first load step
lswrite,1

NLGEOM,1 ! non-linear analysis


! fix keypoint 1
ksel,s,kp,,1
nslk,s
d,all,all,0



! Displace the top, no rotation, (keypoint 19)
ksel,s,kp,,19
nslk,s
d,all,rotz,0
d,all,ux,0
d,all,uy,del2

!write second load step
lswrite,2


lssolve,1,2,1 ! solve the load steps

!finish
```

```
/post1   ! entering post processing


!allsel,all

*get,nele,elem,,num,max

! *** Get Node Number at Keypoint last
KSEL,all                    ! Selecting Keypoint 2
NSLK,s                           ! Selecting the node at KP 2
*GET,nkpl,node,0,num,max         ! Setting the node number to the variable

!writing tables
*dim,mst,table,nele
*dim,mst2,table,nele

*do,dd,1,nele,1
set,1
ESEL,S,ENAME,,beam3
ETABLE,sj,NMISC, 3
*get,msj,Etab,1,elem,dd
*SET,mst(dd),msj
*enddo

*do,dd,1,nele,1
set,2
ESEL,S,ENAME,,beam3
ETABLE,sj2,NMISC, 3
*get,msj2,Etab,2,elem,dd
*SET,mst2(dd),msj2
*enddo

!****************************************

! defining tables to be filled
!*get,sub_st,active,0,solu,ncmss

!*dim,yforce,table,sub_st
!allsel,all

! GET THE FORCE SUM AT THE displaced node

set,1
*GET,forceY,node,nkpl,rf,fy
!*SET,Yforce(DD),forceY

set,2
*GET,forceY2,node,nkpl,rf,fy
!*SET,Yforce(DD),forceY

!ALLSEL,ALL

*VSCFUN,maxsj,max,mst
*VSCFUN,maxsj2,max,mst2
!*VSCFUN,maxf,min,yforce

!************************************

! writing the output file

/output,maxStressandForce.txt
*VWRITE,maxsj
%16.8G
*VWRITE,maxsj2
%16.8G
*VWRITE,forceY
%16.8G
```

```
*VWRITE,forceY2
%16.8G
/output

FINISH

! /POST1
!set,1
!PLETAB,SJ,NOAV
!set,2
!PLETAB,SJ2,NOAV
```